CHALMERS
UNIVERSITY OF TECHNOLOGY

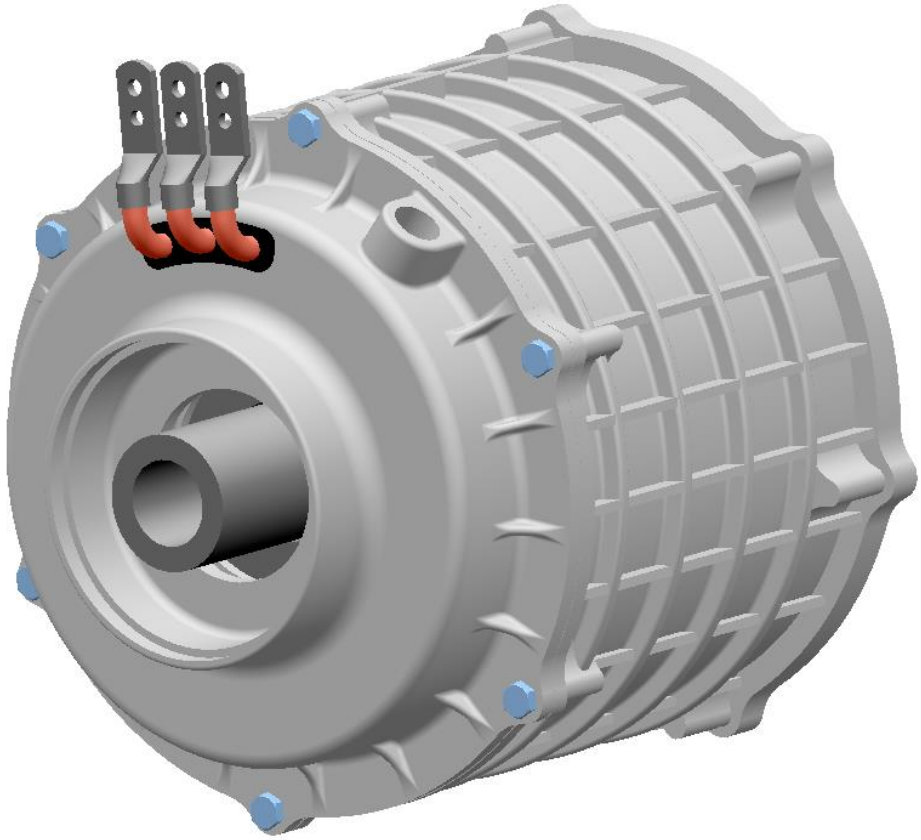

Development and Evaluation of Internal PMSM Cooling for Electrified Vehicles

Master's thesis in Automotive Engineering

Johan Larsson & Martin Lindström

Department of Mechanics and Maritime Sciences
CHALMERS UNIVERSITY OF TECHNOLOGY
Gothenburg, Sweden 2019

MASTER'S THESIS AUTOMOTIVE ENGINEERING

Development and Evaluation of Internal PMSM Cooling for Electrified Vehicles

Johan Larsson & Martin Lindström

Department of Mechanics and Maritime Sciences
Division of Combustion and Propulsion Systems
CHALMERS UNIVERSITY OF TECHNOLOGY
Göteborg, Sweden 2019

Development and Evaluation of Internal PMSM Cooling for Electrified Vehicles
Johan Larsson & Martin Lindström

Master's Thesis 2019:60
Department of Mechanics and Maritime Sciences
Division of Combustion and Propulsion Systems
Chalmers University of Technology
SE-412 96 Göteborg
Sweden
Telephone: + 46 (0)31-772 1000

Cover:
Complete PMSM design with internal cooling.

Department of Mechanics and Maritime Sciences
Göteborg, Sweden 2019-06-18

Development and Evaluation of Internal PMSM Cooling for Electrified Vehicles
Master's thesis in Automotive Engineering
Johan Larsson & Martin Lindström
Department of Mechanics and Maritime Sciences
Division of Combustion and Propulsion Systems
Chalmers University of Technology

Abstract

Electrified vehicles are becoming more common due to tougher emission legislation and customer demands. The need for powerful, compact and efficient electric machines is therefore increasing. The aim in this study was to improve the machine, primarily with regards to these aspects while still keeping it suitable for mass production. To achieve this aim, one area of the machine was identified as having the highest improvement potential, the cooling. This improvement area was chosen after a literature study of the electric machine. An internal cooling concept was developed to replace the existing external cooling jacket solution. Several solutions were considered, the final solution uses hairpin conductors and internal water cooling. The internal cooling solution resulted in a decrease in diameter by approximately 7.9 %, and by using hairpin conductors the length of the machine was reduced by roughly 8.8 %. A CFD analysis was performed which showed an increase in thermal duty by about 70 % while reducing the pressure drop through the system by over 80 % when compared to a conventionally cooled machine. In order to achieve a robust and reliable solution, the development of the sealing as well as insulation solution has been taken into consideration. Furthermore the hairpins are coated to insulate them from the coolant. The improvements to the electric machine opens up for several design choices. The size reduction can make the packaging easier and give room for other components, alternatively, the dimensions of the internal components can be increased to get a higher performance machine with the same outer dimensions as before. An overall more efficient electric machine is beneficial with regards to driving range of the vehicle and in a broader sense, leads to a reduced environmental impact of the vehicles.

Key words: PMSM, electric machine, internal cooling, hairpin, OpenFoam, Helyx, power density, efficiency, pressure drop, convective heat transfer coefficient.

Utveckling och Evaluering av Intern PMSM-kylning för Elektrifierade Fordon
Examensarbete inom Fordonsteknik
Johan Larsson & Martin Lindström
Institutionen för Mekanik och maritima vetenskaper
Avdelningen för förbränning och framdrivningssystem
Chalmers tekniska högskola

Sammanfattning

Elektrifierade fordon blir mer vanliga på grund av striktare emissionslagstiftning och efterfrågan från konsumenter. Därmed ökar behovet av starka, kompakta och effektiva elmaskiner. Syftet med studien var att förbättra maskinen, primärt med avseende på dessa aspekter medan den fortfarande ska vara lämplig för massproduktion. För att uppnå detta identifierades ett område av motorn som visade störst förbättringspotential, kylningen. Detta område valdes baserat på en litteraturstudie av elmaskinen. Ett internt kylkoncept utvecklades för att ersätta den existerande externa kyljackan. Flera koncept övervägdes, den slutgiltiga använder sig av hårnålsledare och intern vattenkylning. Den interna kyllösningen resulterade i en minskad diameter med cirka 7.9 %, och genom att använda hårnålsledare reducerades även maskinens längd med ungefär 8.8 %. En CFD analys av konceptet visade en ökning av värmeöverföringskonstant normaliserad med avseende på area med runt 70 % medan tryckfallet genom systemet reducerades med över 80 % jämfört med en konventionellt kyld maskin. För att uppnå en robust och pålitlig kyllösning har tätning och isolering beaktats. Hårnålarna är belagda med ett isolerande skikt som hindrar att ström leds genom kylvätskan. Förbättringarna av elmaskinen öppnar upp för flera designval. Storleksminskningen kan göra packningen enklare och ge mer utrymme till andra komponenter, alternativt kan motorns interna komponenter öka i dimension för att erhålla en maskin med högre prestanda med samma ytterdimensioner som tidigare. En överlag mer effektiv elmaskin är fördelaktig med hänsyn till räckvidd och ur ett större perspektiv minskar det fordonens miljöpåverkan.

Nyckelord: PMSM, elmotor, intern kylning, hårnål, OpenFoam, Helyx, kraftdensitet, effektivitet, tryckfall, konvektiv värmeöverföringskonstant.

Contents

Acknowledgements

We would like to thank Volvo Car Corporation for the possibility to conduct our thesis. It has been a great experience and it exceeded our already high expectations. Our group at the Propulsion System Geometry Department, 97140, has provided us with great support throughout the project. A special thank you goes out to our two supervisors, Torbjörn Andersson and Raik Orbay. Torbjörn allowed us the freedom to explore the subject and choose our own path while still providing structure and guidance to the project. Raik was an invaluable guide through the cooling analysis process and shared his knowledge with great enthusiasm. Furthermore a warm thank you goes out to the technical experts, Nikitas Sidiropoulos, Joachim Lindström and Aristotelis Babajimopoulos who has dedicated both time and effort to support us. We would also like to thank our examiner Lucien Koopmans at Chalmers University of Technology.

Göteborg March 2019-06-18

Johan Larsson & Martin Lindström

Notations

Roman upper case letters

A	$[m^2]$	Area
B	$[Wb/m^2]$	Peak flux density
B	$[-]$	Additive constant
C_s	$[W/(m^2K^4)]$	Radiation constant for black bodies
D_h	$[m]$	Hydraulic diameter
H	$[A/m]$	Magnetic field strength
I	$[A]$	Current
K_h	$[J/m^3]$	Hysteresis coefficient
Nu	$[-]$	Nusselt number
P_c	$[W]$	Copper power losses
P_e	$[W]$	Eddy power losses
P_h	$[W]$	Hysteresis power losses
$\dot{Q}$	$[W]$	Heat transfer rate
$\dot{Q}_{cond}$	$[W]$	Conductive heat transfer rate
$\dot{Q}_{conv}$	$[W]$	Convective heat transfer rate
$\dot{Q}_{rad}$	$[W]$	Radiative heat transfer rate
R	$[\Omega]$	Resistance
Re	$[-]$	Reynolds number
T	$[K]$	Temperature
T_{in}	$[K]$	Inlet temperature
T_{out}	$[K]$	Outlet temperature
U	$[m/s]$	Velocity
V	$[m/s]$	Velocity
$\boldsymbol{V}$	$[m/s]$	Velocity vector
V_c	$[m^3]$	Magnetic core volume
V_∞	$[m/s]$	Free stream velocity
$\bar{V}$	$[m/s]$	Time mean velocity
$\bar{V}'$	$[m/s]$	Fluctuating velocity

Roman lower case letters

a	$[m]$	Lamination thickness
a	$[m]$	Channel height
b	$[m]$	Channel width
c_P	$[J/K/kg]$	Specific heat
$c_{P,cool}$	$[J/K/kg]$	Specific heat of coolant
f	$[Hz]$	AC frequency
$f_{l/min}$	$[dm^3/min]$	Volumetric flow rate
g	$[m/s^2]$	Gravity
h	$[W/m^2/K]$	Heat transfer coefficient,
k	$[W/m/K]$	Thermal conductivity
k	$[J/kg]$	Turbulence kinetic energy
n	$[-]$	Number of phases
n	$[-]$	Steinmetz coefficient
$nr_{concepts}$	$[-]$	Number of concepts
nr_{opt}	$[-]$	Number of options
p	$[Pa]$	Pressure
$\bar{p}$	$[Pa]$	Mean pressure

$\hat{u}$	$[J]$	Internal energy
u^+	$[-]$	Non-dimensional velocity parallel to the wall
u^*	$[m/s]$	Friction velocity
y^+	$[-]$	Non-dimensional wall distance

Greek upper case letters

Δ	$[-]$	Difference
Φ		Function for viscous-dissipation

Greek lower case letters

ε	$[-]$	Emissivity
κ	$[-]$	Von Karman's constant
μ	$[Pa \cdot s]$	Dynamic viscosity
ν	$[m^2/s]$	Kinematic viscosity
π	$[-]$	Numerical constant
ρ	$[kg/m^3]$	Density
ρ_{cool}	$[kg/m^3]$	Coolant density
σ	$[S/m]$	Electrical conductivity

Other

∇		Nabla operator
∇^2		Laplace operator
$\rho\overline{V}_i' \overline{V}_j'$	$[kg/s^2m]$	Turbulent stresses

List of abbreviations

AC	Alternating current
BEV	Battery electric vehicle
CFD	Computational fluid dynamics
CHT	Conjugate heat transfer
EMF	Electromotive force
HEV	Hybrid electric vehicle
KPI	Key performance indicator
PM	Permanent magnet
PMSM	Permanent magnet synchronous machine
RANS	Reynolds-average Navier-Stokes
SST	Shear stress transport
VCC	Volvo Car Corporation

List of Figures

List of Tables

1 Introduction

In this chapter the background to the study is presented. It also describes the aim of the study followed by the determined research questions as well as the limitations of the scope.

1.1 Background

Electrification is a growing trend within the automotive industry and is one of the most promising strategies to reduce the output of carbon dioxide as well as other emissions. This is necessary not only because of stricter legislation but also due to the increasing demand from customers. Volvo Car Corporation (VCC) is therefore extending their vehicle model offer with a number of electrified powertrains. Battery electric vehicles come with many benefits but they also present new challenges. One of these challenges is packaging. Electric vehicles have entirely different components in the drive train and they therefore require new packaging solutions. There is a finite amount of space available for components in a vehicle and it is in high demand from many different subsystems. The task of positioning the components of a system within limited geometries is complex since the components do not only need to fit, they often have other requirements that limits freedom of placement. If a component needs to be added or is increased in dimension, the surrounding components will need to be moved or redesigned to facilitate the change. Reducing the overall dimensions of a component makes this puzzle a bit easier to solve. One crucial component of a battery electric vehicle (BEV) of which there is a high interest to improve with regards to packaging is the electric machine. Due to the growing interest in electrification, the need for highly efficient, compact and powerful electric motors is higher than ever. Reducing the dimensions while maintaining the performance would increase the design freedom for surrounding geometries allowing for a better overall vehicle.

1.2 Aim

The aim is to improve the permanent magnet electric machine (PMSM) primarily with regards to efficiency and power density while maintaining mass producibility. It should be possible to be implemented in the limited geometries of existing Volvo car sub frames. The project is performed through a literature review of the PMSM and thereafter identifying changes in design/manufacturing concepts which results in improvements in functionality with high potential. These concepts are then evaluated and validated against the current solution which is used as reference.

1.3 Research questions

- What is the major improvement area for the PMSM?
- Which solution shows the most potential?
- What are the potential drawbacks to this solution?
- Will changes in production be required, and if so, in what ways?
- How much is the machine improved compared to the reference?

1.4 Limitations

This project is limited to investigating the electric machine, specifically the PMSM, for implementation in existing Volvo car sub frames. This type is currently used by Volvo and is the industry standard within the automotive sector. The other components of the powertrain will be considered only if required due to changes in the electrical machine. The electric machine will be deeply analysed and investigated with respect to one chosen area of interest, the cooling.

2 Theory

The following chapter contains the supportive information needed for this study. It covers the general basics of the integral parts of the electric machine and its function. Thereafter the principles of fluid dynamics and heat transfer are described.

2.1 PMSM

Tong (2014) describes the PMSM as a highly efficient electric machine that is made up of a rotor and a stator. The rotor is, as the name implies, the rotating part made out of laminated metal and holds the permanent magnets. It is connected to the output shaft and rotates freely inside the stator but without any direct contact between the two components. The stator is the stationary part of the motor that generates rotating electrical fields by running alternating current (AC) through its copper windings. When the stator generates a rotating magnetic field it causes a rotation of the rotor due to the attraction of the permanent magnets poles and corresponding rotating electromagnetic poles generated by the stator. This is the main principle of the PMSM as described by Tong (2014).

2.1.1 Stator lamination stack

The primary purpose of the lamination stack is to enable the magnetic fields and to hold the windings according to Tong (2014). He describes it as built up of several thin sheets made out of electrical steel that are stacked together to form a lamination. Electrical steel is an iron alloy with added silicon that increases both permeability and electrical resistance. The separated sheets in the laminated structure reduces the currents induced into the core due to the insulation of steel sheets which reduces losses as described in Section 2.1.5.1. The lamination can be held together in different ways, bonding with adhesive material is the most common method but welding and other methods are also used (Tong, 2014).

2.1.2 Windings

The purpose of the windings is to generate the rotating electric fields and their function is described in detail by Tong (2014). The copper windings are positioned in such a way that when a three phase alternating current is run through the different coils, a rotating magnetic field is formed. The rotational speed of the magnetic field is determined by the frequency of the alternating current. The windings are most commonly made up of coils of wound insulated copper wire, so called magnet wire. The insulation is made up of a layer of non-conductive material around the wire, preventing short circuits between the tightly packed wires (Tong, 2014). An alternative to traditional windings is the so called hairpin design. Instead of winding one long wire into a coil, several U-shaped pins are placed in the stator core and welded together at the ends to form the closed circuit. These are manufactured to have rectangular cross sections, allowing tight packing of the copper in the stator slots, increasing the so called slot fill ratio or fill factor (England & Ponick, 2019). The slot fill ratio is defined as the percentage of occupied space in the slot by the copper conductors compared to the full volume of the slot. A high fill ratio is generally desired because of the lower resistive losses in the conductors and increased power density (Tong, 2014).

2.1.3 Rotor

The rotor in a PMSM is constructed with a laminated core and firmly secured permanent magnets (PM) positioned in a certain interior or exterior configuration to generate magnetic fields. An example of a typical rotor interior configuration is shown in Figure 2.1. The rotor magnets are separated from one another by an isolating spacing, a so called flux barrier, which is a-magnetic to avoid short circuiting of the magnets (Melkebeek, 2018). The laminated core is typically made out of electrical steel which proves a component with good permeability, thermal conduction and low core losses which is described in Section 2.1.5 (Tong, 2014).

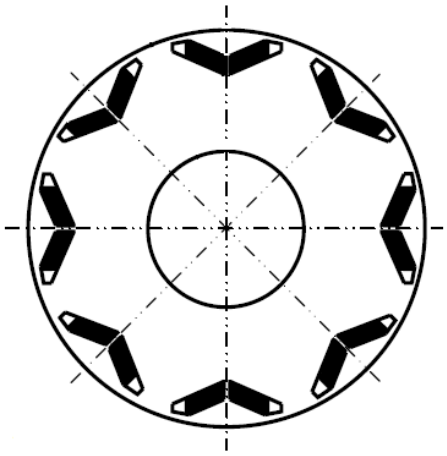

Figure 2.1 Illustration of the PM rotor interior with v-shaped magnet positioning (Tong, 2014).

One issue with using a rotor with PMs is the risk of magnet demagnetization due to high temperatures which causes deterioration in performance. Demagnetization of the PMs effects the electromagnetic characteristics such as reduced residual magnetic flux density which leads to deteriorated torque aspects such as increased variations in torque output, so called torque ripple, and reduced mean torque output as described by Tong (2014). He also says that there are three different levels of demagnetization depending on the temperature and they are either reversible, irreversible (but losses can be recovered) and irreversible which results in a permanent loss in its magnetic properties.

2.1.4 Casing

The rotor and stator assembly is protected by a casing. This casing performs many necessary supporting functions for the machine as Tong (2014) explains hereafter. It holds the stator and supports the rotor shaft with bearings to ensure stable operation of the machine. It also protects the internal components and keeps out particles that can cause failure. The machine is sensitive and even small particles like dust, sand or moisture are harmful. The casing is also designed with mounting points that enables the machine to be installed in the vehicle and it provides structural integrity to the machine. The cooling system is often also incorporated into the casing. The casing is commonly comprised of two parts, an internal and an external casing in between which a closed cooling geometry is formed.

2.1.5 Losses

The electric machine, and the PMSM in particular, has a relatively high efficiency, above 90 % as described by Pyrhonen, el al. (2013). They further say that the losses which are present in the machine have several different causes. In both the stator as the rotor a magnetic material is used as a magnetic core to amplify the magnetic field generated by the copper windings in the stator. The main losses in electrical machines which are run with AC current such as the PMSM are divided into core losses and copper losses (Pyrhonen, et al., 2013). Other examples of losses are mechanical friction in bearings and stray losses in the form of flux leakage and air gap between rotor and stator (Benhaddadi, et al., 2011).

2.1.5.1 Core losses/iron losses

Core losses, which are also called iron losses, are energy dissipation due to parts in the electrical machine experiencing an alternating magnetic flux from the AC current flowing through the stator windings (Pyrhonen, et al., 2013). These correspond to approximately 20-25 % out of the total power losses in an electrical machine (Tong, 2014). Core losses are mainly made up of two types which are called hysteresis and eddy current losses. The losses from eddy currents are proportional to the AC frequency squared while hysteresis losses are frequency proportional which means that heat generation from iron losses increase with higher engine speed (Pyrhonen, et al., 2013). Iron losses are also temperature dependent where each one follows an approximately linear trend. Higher stator and rotor core temperatures yields lower iron losses (Xeu, et al., 2017).

Tong (2014) say that ferromagnetic materials which are positioned inside a magnetic field causes the materials atomic dipoles to align themselves according to the magnetic field. He further states that if this magnetic field is generated through AC current conductor it causes the atomic dipoles to continuously change according to the field and that some of the magnetization is kept due to defects in the crystalline structure of the ferromagnetic material which is called magnetic hysteresis. He determines that when the magnetic field changes it requires some additional energy to align the atomic dipoles to the magnetic fields orientation and this additional energy is called hysteresis losses. The size of the hysteresis power losses, P_h, is described as

$$P_h = K_h V_c B^n f \tag{2.1}$$

where K_h is the material specific hysteresis coefficient, V_c is the volume of the magnetic core, B is the peak flux density, n is the Steinmetz coefficient and f is the AC frequency (Tong, 2014).

In Figure 2.2 the hysteresis loop is shown for two different types of materials where B is the peak magnetic flux density and H is the magnetic force. The hysteresis losses in the materials are proportional to the loop surface (Vukosavic, 2013). As can be seen in the figure, hysteresis losses are higher for a harder magnetic material due to the increased size of the loop area (Tong, 2014). Around 75 % of the total iron losses are made up from hysteresis losses (Pyrhonen, et al., 2013).

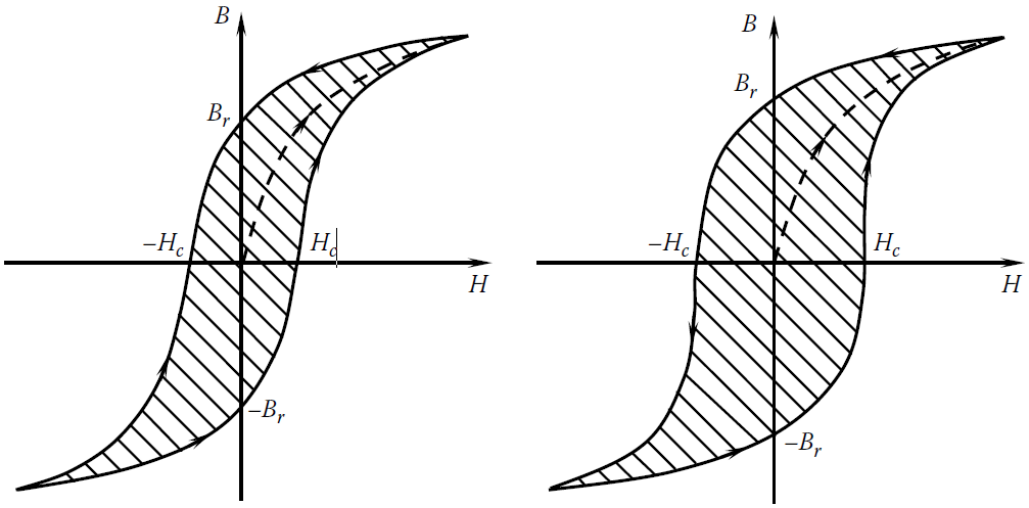

(a) Soft material *(b) Hard material*

Figure 2.2 Two types of magnetic materials magnetization hysteresis loops (Tong, 2014).

Both Tong (2014) and Pyrhonen, et al. (2013) say that introducing an alternating magnetic flux to conductive machine components, mainly stator and rotor, induces electromagnetic force in the form of voltages in the material which causes circulating electrical currents. They further state that these are called eddy currents and through resistance in the material it leads to energy dissipation and heat generation inside the components. Having laminated components such as the stator and rotor rather than a solid piece of metal reduces the effect of eddy currents (Pyrhonen, et al., 2013). The reduction in effect is because the layered construction restrict size of the eddy current circulation into each individual layer, as shown in Figure 2.3, which reduces the overall losses from eddy currents (Tong, 2014).

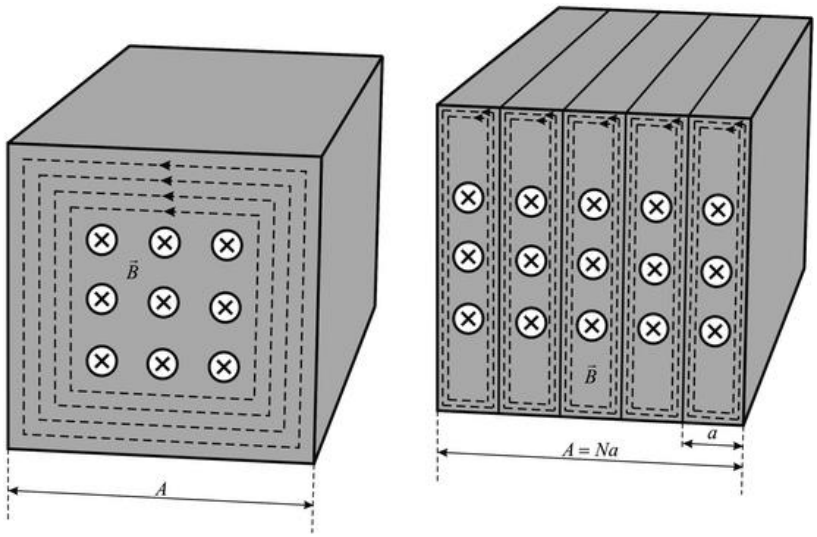

(a) Solid structure *(b) Laminated structure*

Figure 2.3 Eddy currents visualized for different structure types (Vukosavic, 2013).

The power losses from eddy currents, P_e, are according to Tong (2014) expressed as

$$P_e = \frac{\pi^2}{6} V_c B^2 f^2 a^2 \sigma \tag{2.2}$$

where a is the lamination thickness and σ is the electrical conductivity. The equation shows that the eddy currents are squared proportional to both the thickness of the used lamination as well as the AC frequency. This means that the lamination thickness has a significant influence on the size of the eddy current losses and that eddy currents are prevalent at higher engine speeds.

2.1.5.2 Copper losses/resistive losses

Pyrhonen, et al. (2013) says that copper losses, which are also called resistive losses, are caused by heat generated in the copper windings from the electrical resistance in the conductor to the flowing current. They determine the equation for copper power losses, P_c, as

$$P_c = nI^2R \tag{2.3}$$

where I is the current, R is the resistance and n is the number of phases, typically of the three-phase type. This equation shows that the copper losses are proportional to the current squared which means that heat generation in the windings increase with higher motor torque. Furthermore it is described that increased heat generation at higher power levels leads to overheating which is one of the reasons why an EM has a continuous power rating which is lower compared to its maximum.

The resistance in the copper winding is not constant but varies depending on temperature. At elevated temperature the electrical resistivity increases which results in additional heat generation and a lower efficiency (Hussain, et al., 2016). For most electrical machine applications copper losses are considered to be the largest contributor to energy losses except applications which run at high engine speeds (Tong, 2014).

2.1.6 Cooling

When alternating currents are run through the copper windings of the stator, heat is generated. This is due to the copper and core losses described in the previous Section 2.1.5. Tong (2014) explains that in order to prevent damage of the machine and to maintain high continuous power generation, the machine requires cooling. In automotive applications the power demand is high and the machine needs to be able to run for several hours of continuous operation. Passive cooling is not sufficient to keep the operating temperature below the critical limit in these conditions. Tong (2014) further explains that the critical limit is dependent on material properties of the used magnets as well as the winding insulation material. The permanent magnets in the rotor are sensitive to heat and are demagnetized above a certain temperature called the Curie temperature causing the machine to lose its function. The insulating coating on the magnet wires can also be damaged at high temperatures but this temperature is generally higher than the demagnetization temperature of the magnets. In order to prevent damage, the typical PMSM used for the automotive application is therefore either water or oil cooled. Another aspect of the cooling performance is the thermal interface between the components. Epoxy resin and thermal interface materials such as thermal grease are used to improve the thermal conductivity between two bodies. These

materials replaces the air which is a thermal insulator due to its high thermal resistance (Tong, 2014).

A common cooling solution today is external cooling of the machine, meaning that the coolant flows in channels of the housing (Tong, 2014). This solution is called a cooling jacket. The cooling jacket is often made up of an inner and outer casing that form cooling channels between them. Coolant, most often water with additives such as glycol, is then pumped through the channels removing heat from the machine. Tong (2014) explains that the benefits of external cooling are mainly simplicity and reliability. Since the coolant is completely separated from the machine, it does not impact the design of the rotor and stator. The separation also means that the risk of coolant leaking into the machine is very low.

Tong (2014) also describes another cooling method, direct liquid cooling, which means that the machine allows coolant to flow close to or within the active components of the machine, for example in the stator or rotor. The main benefit of this cooling method is that the coolant comes closer to the components that generate heat. Providing cooling at the heat source gives a lower thermal conduction resistance compared to the external cooling and allows for more efficient cooling. The drawback is that the complexity rises and it is also challenging to achieve in a reliable way.

2.2 Heat transfer

Böckh & Wetzel (2012) states that heat transfer of thermal energy occur between two bodies in thermal contact with one another when there is a temperature gradient present. They also say that there are two forms of heat transfer modes called thermal conduction and radiation. A third mode called convection is typically described in literature, however this mode of heat transfer process is dependent on thermal conduction as determined by Böckh & Wetzel (2012).

2.2.1 Conduction

Thermal conduction is created when there is a temperature gradient within a material. Conductive heat transfer rate in static materials depends on the temperature gradient and the properties of the materials (Böckh & Wetzel, 2012). The relation between the thermal conductivity and the rate of heat flow is referred to as Fourier's law of heat conduction (White, 2008). The equation to calculate the thermal conduction heat rate, $\dot{Q}_{cond}$, for a 1-D geometry is

$$\dot{Q}_{cond} = -kA\frac{dT}{dx} \tag{2.4}$$

where k is the thermal conductivity, A is the surface area through which the flux travels and dT is the temperature difference in the heat flux direction, x (Böckh & Wetzel, 2012).

2.2.2 Convection

Thermal convection is a special case of conduction but because of the different ways of calculating the heat transfer it is often regarded as a separate mode. Böckh & Wetzel (2012) describes convection as being divided into two different types. The first one is

called free convection, or buoyancy driven flow, and occurs when a difference in temperature causes a change in density which together with the gravity results in a fluid flow. The other type is forced convection and is created when an external source creates a fluid flow due to a difference in pressure. They further show that the thermal convective heat rate is calculated as

$$\dot{Q}_{conv} = hA\Delta T \tag{2.5}$$

where h is the heat transfer coefficient, A is the surface area and ΔT is the temperature difference between the surface and the fluid.

2.2.3 Radiation

All surfaces and gases with a temperature above absolute zero radiate energy through electromagnetic waves. The energy exchange between two surfaces is created by the difference in temperature. The surface can either be a black, grey or white body. Black body means that the surface absorbs all the radiated energy while a white body reflects all of it. A grey body has an absorption between 0 and 1 which means that it both absorbs and reflects parts of the radiation. The equation for radiative heat rate for a grey body becomes

$$\dot{Q}_{rad} = \varepsilon C_s A \left(\frac{T}{100}\right)^4 \tag{2.6}$$

where ε is the emissivity, C_s is the radiation constant for a black body, A is the surface area and T is the temperature (Böckh & Wetzel, 2012). The heat rate equation is simplified for a black body by using an emissivity equal to 1.

2.3 Fluid mechanics

Within the engineering field the general theory of fluid mechanics is used to describe the fluid as a continuum and its motion based on three basic laws of mechanics. The three basic laws of mechanics, as described by White (2008), are the conservation of mass which is also known as the continuity equation, conservation of linear momentum which is based on Newton's second law and the conservation of energy which is the first law of thermodynamics. He further states that the conservation of mass implies that there are no sources generating additional mass or singularities which extract mass from within the system. This simply means that the mass within a closed system stays constant over time. For a steady incompressible flow the continuity law becomes

$$\boldsymbol{\nabla} \cdot \boldsymbol{V} = 0 \tag{2.7}$$

where $\boldsymbol{\nabla}$ is the nabla operator and $\boldsymbol{V}$ is the velocity vector (White, 2008). For a Newtonian fluid with a constant density and viscosity the linear momentum equations are called the Navier-Stoke equations for incompressible flow as described by White (2008). He shows the form of the equations with the gravity as the only body force as

$$\rho g_i - \boldsymbol{\nabla} \mathrm{p} + \mu \boldsymbol{\nabla}^2 V_i = \rho \frac{dV_i}{dt} \tag{2.8}$$

where ρ is the density, $\boldsymbol{\nabla}^2$ is the Laplace operator, g is the gravitational force, p is the pressure, μ is the dynamic viscosity of the fluid and i is the direction in either x, y or z. He also states that for a Newtonian fluid the energy equation is on the form

$$\rho \frac{d\hat{u}}{dt} + p(\boldsymbol{\nabla} \cdot \boldsymbol{V}) = \boldsymbol{\nabla} \cdot (k \boldsymbol{\nabla} T) + \Phi \tag{2.9}$$

where $\hat{u}$ is the internal energy, k is the coefficient of thermal conductivity and Φ is the function for viscous-dissipation.

Characteristic length is used as a dimension to indicate the size of the system and is for example used in fluid dynamics for the calculation of Reynolds and Nusselt numbers. For a rectangular channel the characteristic length is the hydraulic diameter, D_h, and is calculated as

$$D_h = \frac{2ab}{a+b} \tag{2.10}$$

where a is the channel height and b is the width (Bejan, 2013).

Reynolds number, Re, is a dimensionless number which can be used to roughly estimate the flow behaviour. The Reynolds number needs to be calculated for determination of whether or not the flow in the cooling channel is laminar or turbulent by using the following equation

$$Re = \frac{V_\infty D_h}{\nu} \tag{2.11}$$

where D_h is the hydraulic diameter, V_∞ is the free stream velocity and ν is the fluid viscosity (Bejan, 2013). A value of $Re < 2300$ indicate a laminar flow and $Re > 10^4$ is typical for a flow that is turbulent (Böckh & Wetzel, 2012).

Nusselt number is also described by Bejan (2013) as a dimensionless heat transfer coefficient which is dependent on the Reynolds number, fluid characteristics, heat flux direction and the geometry. He claims that for fully developed laminar flow through a long circular tube with uniform temperature distribution the Nusselt number is 3.66. Böckh and Wetzel say that since the Nusselt number is dependent on the Reynolds number the transition from laminar to turbulent flow results in a discontinuous jump in Nusselt number. They also show that low values below 10 are typical for laminar flow while the values over 100 are typical indications of turbulent flow (Böckh & Wetzel, 2012). For forced convection in a pipe with a fully developed laminar flow the Nusselt number is calculated as

$$Nu = \frac{hD_h}{k} \tag{2.12}$$

where h is the convective heat transfer coefficient and k is the fluids thermal conductivity (Bejan, 2013). The Nusselt is therefore the ratio between the convective and conductive conductive heat transfer and can be used as an indicator of heat transfer performance.

2.3.1 CFD

Computational Fluid Dynamics (CFD) is as the name implies a computer based method for analysing fluid flow. It allows for the solving of complex fluid dynamics problems and is therefore used widely in the industry to analyse a broad range of areas relating to fluid flow. It does however have its limitations when it comes to simulation of quick variations of velocities and pressures in time and space due to turbulence as described by White (2008). He further says that by analysing the average and fluctuating variables of the flow over a period that is longer than the variations the Reynolds-averaged Navier-Stokes equations (RANS) can be derived for turbulence modelling

from equation (2.7) and (2.8). The RANS equations for an incompressible flow and with gravity as the only body force are derived according to White (2008) as

$$\boldsymbol{\nabla} \cdot \bar{\boldsymbol{V}} = 0 \tag{2.13}$$

$$\rho \frac{d\bar{V}_i}{dt} = -\boldsymbol{\nabla}\bar{p} + \rho g_i + \mu \boldsymbol{\nabla}^2 \bar{V}_i - \rho \boldsymbol{\nabla} \cdot \overline{\mathrm{V}}_{\mathrm{i}}' \, \bar{V}_j' \tag{2.14}$$

where $\bar{V}$ is the time mean velocity, $\bar{V}'$ is the fluctuating velocity, $\bar{p}$ is the mean pressure and the $\rho \overline{\mathrm{V}}_i' \, \overline{\mathrm{V}}_j'$ terms are the turbulent stresses creating a closure problem. These turbulent stresses needs to be solved using turbulence models such as for example Menters shear stress transport (SST) *k-ω* model to compute the turbulent flows with RANS as described by Vertsteeg and Malalasekera (2007). They describe the model as a combination of the *k-ω* and *k-ε* models for different parts of the boundary layer. More specifically that the *k-ε* models is used for the turbulent flow far away from the wall but due to its poor performance in the near-wall region the model is transformed to the *k-ω* model in this region.

Having a solid boundary, such as a wall, influences the typically inertia-dominated flow by introducing a small layer near the wall in which the viscous forces have a large influence (Vertsteeg & Malalasekera, 2007). The various parts of the layer are described by White (2008) with Figure 2.4 where he shows the inner, overlap and the outer layers.

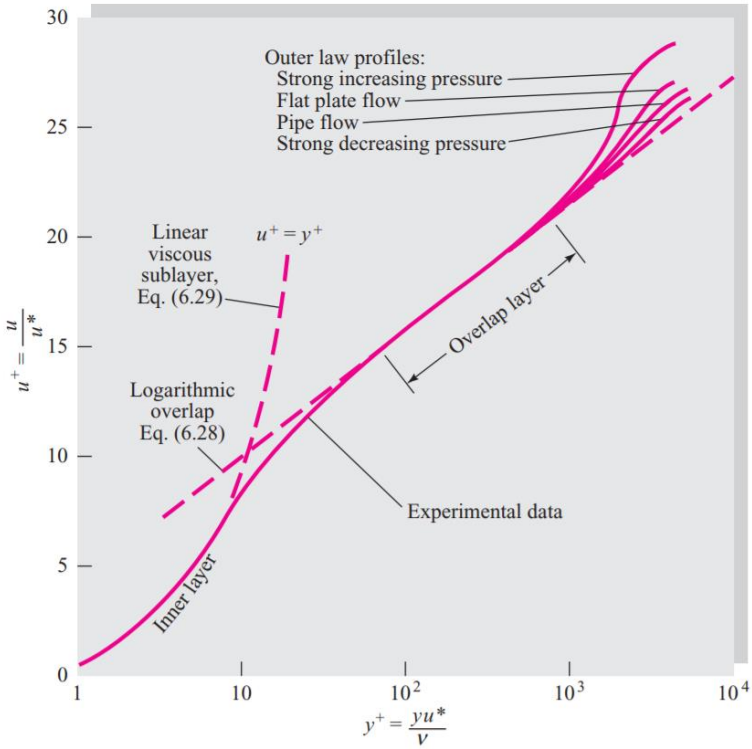

Figure 2.4 Overlapping layer laws of turbulent flows velocity profiles (White, 2008).

He further says that the law of the wall follows the linear viscous sub-layer from the wall up to the non-dimensional wall distance $y^+ \leq 5$ as

$$y^+ = \frac{yu^*}{\nu} \tag{2.15}$$

where u^* is the friction velocity, ν is the kinematic viscosity and y is the distance to the outer layer edge. It then arcs to merge at approximately $y^+ = 30$ with the logarithmic overlap layer law, which is valid in the log-law region $30 < y^+ < 500$, on the form

$$u^+ = \frac{1}{\kappa}\ln(y^+) + B \tag{2.16}$$

where κ is the von Karman's constant and B is the additive constant (White, 2008) (Vertsteeg & Malalasekera, 2007). For a specific node with $y^+ \leq 11.63$, it can be considered that the near wall flow is laminar while for $y^+ \geq 11.63$ it's in the log-law region of the turbulent boundary layer (Vertsteeg & Malalasekera, 2007).

Vertsteeg and Malalasekera (2007) say that by numerically calculating the two sides of the momentum equations with under-relaxed velocities and pressures the results typically show a difference between the two sides, a so called residual. Under-relaxed factors are used to reduce oscillations and improve the stability of the computations. They further say that if the velocity and pressure fields are calculated in an iterative process and the sum of the absolute residuals reduce it means that the solution is converging. However if the residuals are increasing it means that result is diverging away from the true solution. In the best of situations the residuals are removed entirely, however due to limitations in computer power and computation time this is not possible. There is therefore a balance between the accuracy of the solution and the required computation time. The solution is considered as converged when the sum of the absolute residuals are lower than a predetermined number, typically on a scale of approximately 10^{-5} (Vertsteeg & Malalasekera, 2007).

3 Method

The following chapter describes the scientific method process carried out during the project from initial idea to completed concept design as shown in Figure 3.1. The process starts in a product development phase by describing how an initial literature study is used to determine the main focus area for the project as improving cooling of the EM. This is followed by stages in concept generation, evaluation and selection. Once the chosen concept has been selected the following sections describe the process of performing CFD simulations to determine the cooling performance of the design.

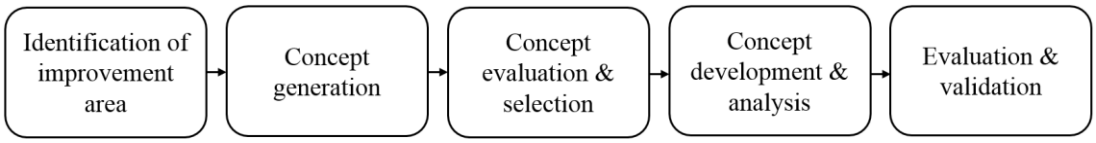

Figure 3.1 Method workflow process

Once the CFD simulations have been performed the focus shifts to describing the method of making the concept realizable in terms of electric insulation, sealing and overall producibility. The last two steps in the process are evaluation of the concept in terms of key performance indicators (KPI) and validation of the results in comparison to a reference solution.

3.1 Identification of improvement area

There are many areas of the PMSM that can be optimized in order to achieve the aim of the project. In order to get a good understanding of the system and the areas that show the highest potential for improvement, a literature review was performed. Resources from the Chalmers library as well as research articles were used together with input from both engineers at Volvo and professors at Chalmers. The initial study also included gathering of information regarding the current and future production methods of the PMSM. After the literature study, one improvement area was identified as having the greatest potential. The evaluation of improvement potential was not performed in a quantitative way, instead the approach was relativistic. There were no calculations performed of precisely how much each area could be improved, instead they were compared to each other. This area was chosen based on how much it could potentially improve the machine with respect to a number of identified criteria of varying degree of importance. The criteria and their importance can be seen in Table 3.1. The main criteria are dimensions (size), efficiency, power and possibility to mass produce. Below those are parameters which were weighted lower compared to the primary parameters but large compromises cannot be made. A number of less important criteria also needs to be considered but they are the lowest weighted and compromises can be made. The weighting of these criteria mirror the overall goal for this project and were determined together with a supervisor in the initial stage of the project.

Table 3.1 Priority list of the different evaluation criteria.

Criteria	Priority
Dimensions (size)	High
Efficiency	High
Power	High
Possibility to mass produce	High
Quality	Medium
Manufacturing time	Medium
Cost	Medium
Environmental aspects	Medium/Low
Complexity	Low
Weight	Low
Structural properties	Low

3.2 Product development

In this section the processes of concept generation, evaluation and determination within product development is described. The theory is based on the processes and methods as described in detail by Johannesson, et al. (2004) and Mital, et al. (2008). When it comes to product development Johannesson, et al. (2004) say that the methods and theories are used to increase the workload at early stages in the project to avoid issues at a later stage due to early mistakes. As Project Management Institute (2008) shows in Figure 3.2 the freedom to perform changes in a project diminishes later in the process with increasing costs.

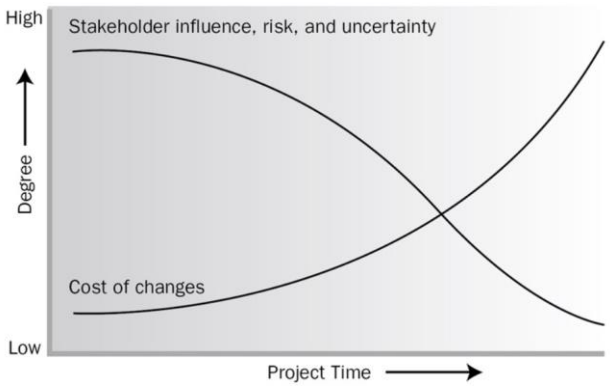

Figure 3.2 Cost and influence of performing changes over the projects duration (Project Management Institute, 2008)

In the following sections the steps of this systematic approach are presented in detail ranging from initial concept ideas to concept evaluation.

3.2.1 Concept generation

The first step in product development after defining the priorities of the various criteria is the concept generation phase. This phase has been performed by brainstorming, discussing with engineers, looking at various patents within the area and taking inspiration from other industries. Tools such as a morphological matrix has also been

utilized in order to ensure that a broad range of concepts are found. This process was repeated a number of times as new ideas were formed. The phase, as described by Johannesson, et al. (2004), uses a structured and systematic approach to generate concept solutions which cover all potential solutions as well as fulfil the predefined requirements.

3.2.1.1 Brainstorming

The typical first step in concept generation is to perform a method called brainstorming. Brainstorming, as described by Mital, et al. (2008), is a group activity in which people of different backgrounds come together to generate a large number of concept ideas, regardless of how practical or impractical they may be. This is done to effectively utilize the combined creativity of the group. The main rules to uphold during a brainstorming session according to Johannesson, et al. (2004) are to withhold any negative critique or belittlement of an idea and not to process the concepts until after the session ends. All kind of ideas are appreciated because even though they might seem impossible to realize the very thought of them can function as a springboard to other innovative ideas (Mital, et al., 2008). Mital, et al. (2008) says that the brainstorming session is usually initialized by an introduction to the problem, offering some typical solution alternatives and a description of the session rules described above. The session is conducted as such that the group come up with generated ideas in an iterative fashion through a person who is the session moderator. The concepts are then discussed within the group during which some of the concepts can be disregarded.

Based on these guidelines, brainstorming sessions were initiated and performed by the project group to generate concepts that fulfil the aim of the project. The brainstorming phase started with an individual session where the project members stated as many solutions as possible without the influence of anyone else. Each member wrote down short descriptions of the concept idea on their own list. After the individual sessions, a joint session was performed where the ideas were shared between the members. After going through the individual lists, a joint effort was made to build on each other's suggestions and spawn new ones with the inspiration from what had been heard.

Once the brainstorming session within the project group was performed, the same methodology was scaled up to involve the members of the department, approximately 12 more people. This hour long session started with 10 minutes of introduction to the problem to make sure that all participants had the required information. After that, the group was given approximately 25 minutes to generate ideas individually. When that was done, all participants shared their solutions and the session opened up for group discussions and further brainstorming in a joint fashion.

3.2.1.2 Concept combination

A morphological matrix, as described by Mital, et al. (2008) can be used for concept generation purposes by dividing the system into its sub-functions. Each one of the sub-functions can then have several different design choices as sub-solutions to solve that specific function. The matrix is formed by placing the identified sub-functions in the leftmost column and the corresponding sub-solutions as rows to form the matrix, as seen in Figure 3.3. By combining an available sub-solution for each sub-function new concepts can be generated. This procedure allows for clear visualization and determination of all potential concepts (Mital, et al., 2008).

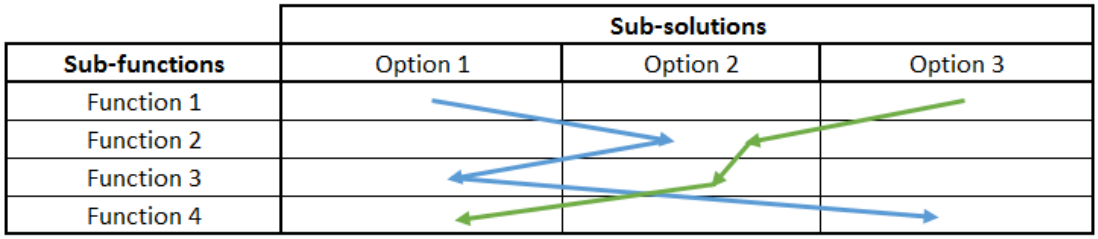

Figure 3.3 Schematic morphological matrix with two paths to create two concepts.

The goal of using a morphological matrix is according Johannesson, et al. (2004) to generate as many realistic concept solutions as possible that meet the predefined requirements.

The morphological matrix gives an overview of all areas relevant to the cooling concept along with all found design options for each area. A number of different design areas have been identified for the overall cooling solutions of the electric machine, these form the first column as functions in the morphological matrix. Each function can be designed in several different ways. The concept results from the brainstorming session are broken down and used as input into the morphological matrix to form the options for each function. When the matrix is complete, an option can be chosen from each function to form a complete concept. Some options are however not possible to combine and many are not suitable to combine. The combination process has been performed systematically starting with option 1 of all areas and then progressing through the full solution space. It has been performed with performance in mind and therefore only resulted in full concepts that were deemed worthy of further investigation.

3.2.2 Concept evaluation and selection

In product development, different methodologies are used in order to choose and improve different types of concepts. A clear work procedure is required as the amount of work in evaluating the large number of combined complete concepts generated from the morphological matrix increase quickly with additional of more sub-solutions. The theoretical amount of complete concepts that can be formed is expressed as the number of options for sub-function 1 multiplied by the number of options for sub-function 2 and so on as expressed as

$$nr_{concepts} = nr_{opt_{F1}} \cdot nr_{opt_{F2}} \cdot \ldots \cdot nr_{opt_{Fn}} \tag{3.1}$$

This determination process can be performed by using a weighting matrix in combination with a weighted Pugh matrix.

3.2.2.1 Weighted Pugh matrix

To achieve a more technical method in determining the priorities of different criteria a weighting matrix, which is designed to reduce the subjective influence, is used. This method is described in detail by Johannesson, et al. (2004) and they claim that there are no entirely objective methods for creating criteria weights, however the subjective influence in the process can be minimized. They further say that this can be achieved by the use of a weighting matrix that compares the importance of the different criteria to each other row by row in a structural fashion, as shown in Figure 3.4. By grading the different criteria against one another on a scale of 0, 0.5 and 1 followed by adding them

together a weighting sum can be calculated. The three different values corresponds to the criteria importance where 1 is higher importance, 0.5 is equal importance and 0 mean lower importance. These weighting sums can be used as weights for each criteria in the matrix. Another way of achieving weighting values is by calculating the percentages of each criterion based on the total sum. These percentages are then graded from 1 to the number of different criteria and then assigned weight values based on the percentages. If two criteria have the same percentages, the lower weight value is used. All three of the sum, percentage of the total and the weight values can be used for the criteria weighting.

	A	B	C	D	E	F	Sum	%	Weight
A		1	0,5	1	1	1	4,5	30	5
B	0		0	1	1	1	3	20	4
C	0,5	1		1	1	1	4,5	30	5
D	0	0	0		0	1	1	6,7	2
E	0	0	0	1		0,5	1,5	10	3
F	0	0	0	0	0,5		0,5	3,3	1
							15		

Figure 3.4 Schematic weighting matrix.

By adding the different criteria from Table 3.1 into the matrix the importance of each criterion is weighted against the rest to achieve weight values which are more detailed compared to the earlier assigned priority order. Due to their close relation, the two criteria *possibility to mass produce* and *manufacturing time* are combined for use in the weighting matrix. In the weighting matrix it is the weight value that is determined to be used further on in the Pugh matrix. The sum values will however still be used to validate that the total score in the Pugh matrix doesn't change significantly depending on the chosen method.

A Pugh matrix is used in an iterative form to assess and compare different ideas relative to a reference in order to obtain an objective and transparent work procedure. It is typically used for concept assessment based on a functional specification (Silverstein, et al., 2012). The procedure in creating a Pugh matrix, shown in Figure 3.5, is by adding the criteria from the functional specification as a column on the furthest left which creates one specific row per criteria. The different concepts are then listed on a row forming designated columns for the concepts which finishes the matrix shape (Vivek, 2017). The used criteria are the design criteria specified in the weighting matrix. The next step is choosing one of the concepts as the reference to which all other concepts will be compared and placing it on the furthest left on the concept row. Thereafter the concepts are compared to the reference for each criteria with either a plus if it it's better, negative if it's worse or zero if there is little difference (Silverstein, et al., 2012).

	Concepts					
Criteria:	**Reference**	**1**	**2**	**3**	**4**	**5**
Criteria 1	0	+	-	-	0	-
Criteria 2	0	-	0	-	+	-
Criteria 3	0	0	+	0	0	+
Criteria 4	0	+	-	0	-	+
Criteria 5	0	0	-	+	0	0
Criteria 6	0	+	-	0	+	+
Criteria 7	0	+	-	0	0	0
Sum +	0	4	1	1	2	3
Sum -	0	1	5	2	1	2
Total Score	0	3	-4	-1	1	1

Figure 3.5 Schematic Pugh matrix.

Important to note is however that in the standard Pugh matrix, shown in Figure 3.5, all the functional specification parameters are weighted the same, which means that they are all equally important (Powell & Buede, 2012). In real world applications however all parameters do typically not have the same importance and the Pugh matrix needs to be changed to take this into consideration. Therefore a weighted Pugh diagram is created by using weight values and adding them as a new column in the diagram to function as a criteria multiplier (Vivek, 2017). This is done by using the weight values of the different criteria generated by the previously described weighting matrix. The first iteration of the Pugh matrix is performed with the current solution as reference. The concepts which receive a low or negative score compared to the current solution are removed during the process. Based on the first iteration a new reference is determined from the highest scoring concepts, depending on its improvement potential, to be used in the second iteration. From the results of the second iteration a selection of unique concepts are selected for further evaluation.

3.2.2.2 Evaluation with experts

From the Pugh matrices the most promising determined concepts within a specific area are determined in collaboration with engineers at VCC who are technical experts within the fields of electrical machines and cooling. The expert concept evaluation is performed in an interview format with relevant engineers to receive their opinion and verdict whether the concepts are feasible. A presentation of the concepts is performed to describe the different solutions and their potential benefits and downsides. The technical experts were then asked to provide their unbiased opinion on what concepts they consider to have the highest potential. Based on this feedback a selection of a cooling concept was performed.

3.3 Concept development and analysis

By performing an analysis of the selected concept, there are certain changes in the construction components which are identified as important for the design evaluation. These components and their interaction with one another are then in-depth analysed to allow for the creation of a geometrical representation. The concept designs are then created using the computer-aided design tool, Catia V5.

The main components which require redesign are the housing, stator, insulation, hairpins, three-phase connection and the inlet/outlet cooling geometries. Therefore

components such as axle and rotor remain unchanged. Once the components are constructed a CAD assembly is created to combine them into a finished product. The assembly is then saved in a STP format which can be used as input in ANSA version 19.0.1 for further analysis.

3.3.1 CFD

In order to evaluate the performance of the cooling concept, an analysis of heat transfer and pressure drop has been performed. Since no actual testing is possible considering the time scope of this study, CFD simulations have been chosen to investigate the performance. Compared to physical testing it is both cost and time effective. The main purpose of the CFD simulations is to verify that the general principle of the concept is sound, not to optimize the design fully. The method used follows common industry practice.

A number of different CAD geometries has been simulated in OpenFOAM, more specifically Helyx V3.1.0 from ENGYS which is a full 3D Navier-Stokes solver. The simulation results have been used to improve the design of the concept in an iterative way but also to compare the performance to existing solutions. An overview of the CFD work process can be seen in Figure 3.6. A detailed description of the processes will follow in the sections below.

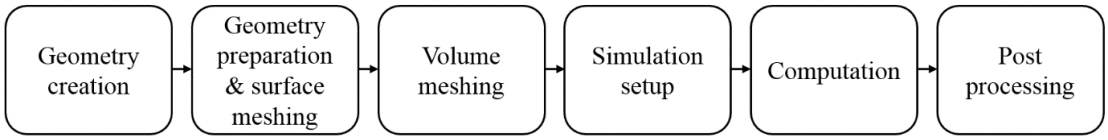

Figure 3.6 CFD work process

3.3.1.1 Geometry creation

The work process of this CFD development phase starts with creating or changing geometries in Catia V5 that represent the physical objects that need to be investigated. An initial simulation of the base geometry was performed that would form the reference. Changing the geometry and running new simulations gives the ability to see if the new geometry is an improvement or not as well as how big of a difference the change in geometry has. In order to be able to tell how a certain change in geometry affects the performance, only one change will be made at a time and will always be based on the base geometry. When certain geometrical changes are shown to improve the behaviour individually, they are combined and analysed in order to verify the combined cooling geometry. Combining two individual geometrical improvements does not always mean that the combination will work better which is why a complete simulation must be run as well.

The two geometrical aspects investigated in this study are the inlet/outlet directions and channel geometry. There are other degrees of freedom of this concept such as inlet and outlet positions, inlet and outlet cross sectional shapes and areas and several more. These aspects will not be investigated.

3.3.1.2 Geometry preparation & surface meshing

The CAD geometry is imported into ANSA Version 19.1.0 in order to generate a surface mesh. Before meshing, the geometry needs to be sealed at the inlet and the outlet. Sealing the geometry is necessary in order to be able to generate an internal volume mesh. The surfaces that seal the inlet and outlet are also used as surfaces on which to apply the inlet and outlet boundary conditions later on in the process. The next step is to assign the correct part names to the components in the geometry and group them together. This allows for a simplified simulation setup and it provides the ability to apply the same simulation scripts to all simulated CAD iterations. After that, a surface mesh of the geometry can be generated. Surface meshing is a necessity in order to generate the volume mesh of the internal volume.

3.3.1.3 Volume meshing

At this stage, the fluid volume is divided into discrete parts. The size and shape of the created mesh influences the result of the simulation, a course mesh will not be able to describe the flow phenomena as well as a finer mesh would, as described by Vertsteeg & Malalasekera (2007). They further say that the drawback of having a fine mesh is that the solving will be more computationally demanding. Ideally the mesh should therefore only be fine enough to be able to give the proper result. Different regions of the mesh might require a finer mesh than others. This is because large variations can occur from point to point in some regions of the flow while other regions experience relatively small changes (Vertsteeg & Malalasekera, 2007). Instead of setting a finer mesh size in the entire domain, refinements can be set where needed. There are several different ways to achieve these refinements in OpenFOAM. It can be done by setting refinement on surfaces that divides the cells closest to the surface of interest into several smaller cells. Another method is to define a number of layers, the layer closest to the surface of interest consists of very fine cells, the next layer is slightly coarser and so on until the base mesh size is reached. Alternatively, certain regions in the domain can be refined using refinement volumes that are meshed in higher detail. If the required mesh size to properly calculate a certain flow field is not known, a mesh study can be performed where finer and finer mesh sizes are tested until the results from the simulations converge (Vertsteeg & Malalasekera, 2007). The volume cells can be set to take the shape of tetrahedral, hexagonal or polyhedral volumes.

The volume mesh used in all simulations is hexa-dominant and is generated using the meshing tool helyxHexMesh in Helyx with a base mesh size of 0.64 mm. A mesh refinement that splits each cell into several smaller cells has been applied where required by using a surface refinement, as seen on for example the hairpins in Figure 3.7. The surface refinement was necessary in order to get the desired mesh quality. This mesh definition was determined to be sufficient to capture the flow phenomena after a brief mesh study was performed.

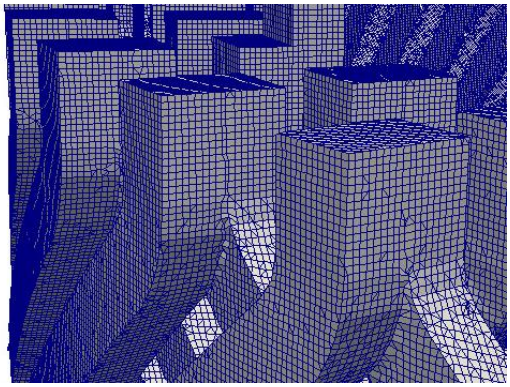

Figure 3.7 Illustration of the fluid volume mesh on the hairpin end-region surface.

The used mesh settings gave roughly 16 million cells in the simulations, with a slight variation between the different simulations. Figure 3.8 illustrates the mesh refinement principle used.

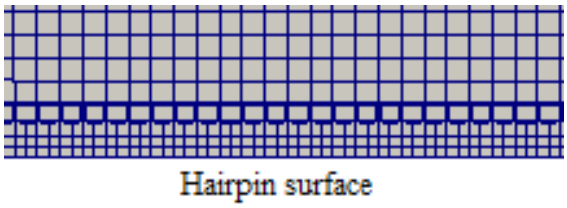

Figure 3.8 Illustration of the coolant volume mesh refinement.

The volume meshing, simulation setup and computation is performed through a script. Having these processes automated is not only very time saving but also prevents manual mistakes that can occur during these steps. The script also handles logging of the processes in order to be able to view and resolve issues in the process.

3.3.1.4 Simulation setup

The simulation setup step is where aspects such as fluid properties and boundary conditions are specified. The flow will vary significantly depending on the fluid, therefore properties such as density, viscosity, specific heat capacity and so on should be defined to accurately mirror the real world case. The coolant properties used in the simulations corresponds to a 50/50 water glycol mix at 313.15 K and are taken from Kumar (2018), see Table 3.2.

Table 3.2 Coolant properties.

Property	Value	Unit
Density, ρ	1069	kg/m^3
Dynamic viscosity, μ	0.00257	$Pa \cdot s$
kinematic viscosity, ν (water)	1.0038e-6	m^2/s
Specific heat, c_P	3340.0	$J/(kg \cdot K)$
Thermal conductivity, k	0.398	W/mK

Boundary conditions define what the flow will be subjected to at the boundaries of the domain (Vertsteeg & Malalasekera, 2007). They can be defined as walls with no slip, which means that the flow will have zero velocity relative to the wall. The full slip condition on the other hand does not decrease the flow speed at the boundary but instead

allows a flow velocity against the wall. In a domain, certain surfaces can be defined with inlet boundary conditions, often with a set flow velocity, volume flow or mass flow according to Vertsteeg and Malalasekera (2007). They further state that the outlets are also specified, often with a set pressure and that other boundary conditions such as wall temperatures or heat transfer can also be defined. The aim is always to mimic the real case to the largest possible extent. The parameters used in all simulations performed can be seen in Table 3.3. These values have been set in order to be representative of what is commonly seen in hybrid electric vehicles (HEVs) today with the help of industry professionals. The inlet temperature is highly dependent on the surrounding system and 70 °C is on the higher end of the scale of what is typically seen. All simulations are performed using the same parameters, the only thing to change between the simulations is the motor geometry.

Table 3.3 CFD design parameters.

Parameters	Value
Coolant inlet velocity $[m/s]$	0.424
Coolant volume flow $[dm^3/min]$	8
Convective heat flux $[W]$	3000
Inlet coolant temperature $[K]$	343
Initial global temperature $[K]$	340

The simulation setup uses a constant inlet velocity based on a representative mass flow and the cross sectional area of the inlet. A constant pressure is set for the outlet. The heat generation is applied by setting a convective heat flux to the heat generating components in contact with the coolant. Furthermore heat transfer in the form of radiation is not considered in the simulation setup as its influence is considered to be negligible. The amount of heat generated is set to represent an operating point corresponding to a high torque demand at low to moderate speeds on the continuous power curve based on a mapping of a representative PMSM of the same power output and dimensions. This operating point was chosen as it represents the limits of the machines durability during continuous operation due to overheating of the conductor insulation.

3.3.1.5 Computation

When the case has been pre-processed it is ready for solving. In this step, the flow phenomena of interest are solved. The governing equations are the Navier-Stokes equations which are solved in three dimensions. The physical flow phenomena are highly complex as well as non-linear, requiring iterative solutions (Vertsteeg & Malalasekera, 2007). In order to properly represent the real flow situation, the different phenomena that are present needs to be accounted for during solving. Models that account for turbulence, heat transfer and so on should be included if the phenomena are present in the case. The case is run using the buoyantBoussinesqSimple solver from the OpenFOAM-Helyx toolbox. This solver allows simulations in steady state under incompressible conditions. Incompressible conditions is a reasonable approximation for a water/glycol coolant in typical pressure conditions. It incorporates turbulence modelling using Reynolds-averaged Navier–Stokes (RANS) and also takes into account buoyancy (Boussinesq's approximation) and non-isothermal conditions. All of the above have been used in the performed simulations. Since buoyancy driven flows

require a model for minor changes in density and the solver is incompressible, the Boussinesq approximation is used to handle the slight density changes.

The turbulence model used is k-ω SST. The reason that this turbulence model was chosen is that it is usual VCC practice for internal flows since it more accurately determines the flow behaviour with regards to shear stresses. Turbulence is a very significant aspect for heat transfer and needs to be considered in order to get trustworthy results. The simulations performed are steady state, meaning that the flow field is solved throughout a number of iterations until convergence is reached. The level of convergence is determined by analysing the residuals of the simulation. The simulation can be considered as converged when the residuals no longer fluctuate significantly and when they have reached a sufficiently low level. For this study that level was at maximum 10^{-2}. In order to achieve a good convergence, initial fields are obtained from a potential flow solution using the potentialFoam solver. This allows the flow field to start from reasonable field magnitudes instead of using user assigned uniform values. The simulations in this study have been performed for 3000 iterations which allowed for properly converged results.

The computations are run on the VCC high performance computing resources, allowing for fully parallel computations using 490 cores.

3.3.1.6 Post processing

When a solution has been generated, the results need to be viewable and understandable for the user. Post processing allows for output of the numerical data of interest as well as visualisation of the flow behaviours, it can display temperatures, velocities, pressures, streamlines etc. for the entire domain (Vertsteeg & Malalasekera, 2007). The post processing has been scripted to output the desired parameters. The parameters of interest in this study are the mean outlet temperature, hairpin surface temperature, pressure drop and convective heat transfer coefficient. The design variations can be compared to each other based on these KPIs. The pressure drop is defined as the difference between the average inlet and outlet pressure. From the post processed results the calculated pressure is normalized based on the density of the fluid with the unit $[Pa\, m^3/kg]$. In incompressible flow calculations the standard outputs are kinematic which means that they are normalized by the density of the fluid. These values are therefore converted to receive a non-normalized pressure drop in the SI-unit Pascal.

The temperature difference between the inlet and outlet, ΔT, can be determined by numerical analytical calculations when all the involved parameters are predefined, according to

$$\Delta T = \dot{Q} / \left(\rho_{cool} c_{P,cool} \frac{f_{l/min}}{60 \cdot 10^3} \right) \tag{3.2}$$

where $\dot{Q}$ is the heat rate, $f_{l/min}$ is the volumetric flow rate in litres per minute, ρ_{cool} is the coolant density and $c_{P,cool}$ is the specific heat (JinXin, et al., 2010). This analytically calculated temperature difference is then used for validation of the simulated results accuracy. Other parameters used for simulation validation are the value of y^+, the outlets patch integrated volumetric flow rate and residual plot to determine the iterative convergence.

The convective heat transfer coefficient, h, is calculated by using equation (2.5) in Section 2.2.2 and rewriting it on the following form

$$h = \frac{\dot{Q}}{A\Delta T} \tag{3.3}$$

where A is the wetted surface area and ΔT is the difference between the average surface temperature of the heat generating components and the average fluid temperature. The average fluid temperature is derived as the inlet temperature plus half of the temperature difference between the inlet and outlet. The thermal duty is calculated by multiplying the convective heat transfer coefficient with the wetted surface area transferring heat. The thermal duty is therefore an area independent value which can be used to compare the heat transfer performance of different cooling concepts.

For the concept design the hydraulic diameter, Reynolds and Nusselt numbers in the channels are calculated according to equations (2.10) – (2.12) in Section 2.3. The hydraulic diameter is calculated based on the width and height of a channel in the CAD geometry. The Reynolds and Nusselt numbers are calculated with the coolant properties in Table 3.2 together with the flow velocity and convective heat transfer coefficient derived from the CFD results. The used free stream flow velocity is the velocity seen in the centre of the channel in the CFD simulations.

3.3.1.7 Conjugate heat transfer

In order to better estimate the cooling performance of the concept, a more detailed CFD simulation was performed for the base design that included modelling of conjugate heat transfer (CHT). This model was set up as an extension of the previous CFD simulations to provide a more accurate representation of the real case. It is performed in a similar fashion as the previous simulations but an additional volume mesh of the hairpins is created. Only the hairpins were meshed in addition to the coolant in order to maintain as low complexity as possible. In order to achieve this setup, the hairpin geometry had to be simplified so that the entire hairpin assembly is connected to form one volume domain. This was done by adding a ring at one of the end region sides where it's typically connected to the inverter connection. The hairpins were further altered by removing the surfaces which overlap with other surfaces. A base mesh size of 0.7 mm has been used for both meshes and similar surface refinements was applied. The hairpin mesh and the fluid mesh communicate over their common boundaries and allows them to influence one another. The same total heat effect of 3000 W was evenly distributed in the volume of the hairpin mesh and replaces the previous boundary condition of a set wall heat flux. The applied heat effect increases the temperature of the hairpins and the temperature difference between the hairpins and coolant gives rise to heat transfer.

3.3.2 Insulation and sealing

By analysing the created CAD geometry there are specific areas which require special attention when it comes to reliability and functionality which can be identified. The two main issues that require solving are sealing of the fluid volume as well as electrical insulation of the current carrying components.

A proper investigation of the geometry was performed to identify which surfaces require sealing. This was performed by identifying the gaps between the different

components which make up the walls for the fluid volume enclosure. The sealing method is dependent on geometry, material and temperature gradients and based on these parameters an appropriate sealing method was chosen and designed for each interface. Providing a sufficient sealing of the cooling geometry is key to avoid coolant leakage which can cause short circuit and corresponding machine failure. For interfaces where no conventional sealing method is applicable, additional ones will be investigated which generate new sealing concepts.

Additionally an analysis was performed of the individual insulation coating thickness on the electrically conducting hairpins. This was done to determine a rough estimation of how thick coating is required to avoid short circuits over the entire lifespan of the electric machine.

3.4 Evaluation and validation

There are several criteria which require evaluation to determine the performance of the new electric machine concept design. Two of the key performance criteria are the electric machines efficiency and maximum continuous power output. This is performed by analysing previous performed work on similar cooling concepts to show the performance improvement for these two criteria over the cooling jacket solution.

Furthermore by examining the created CAD geometry and comparing it to a reference solution the size and packability of the design can be evaluated and validated. When it comes to size, the two main dimensions that are investigated are the axial and radial length of the electric machine. The geometry of the machine is also analysed when it comes to packability to determine the bulkiness of the new design and whether or not it may lead to issues with implementation into the existing predefined sub-frame.

To evaluate the mass producibility of the product the manufacturing process is analysed. The evaluation of the manufacturing process also includes the sealing procedure of the interfaces between the different components. The analysis of the manufacturing process was then used with the reference process to show the potentially positive and negative characteristics of the new design.

From the CFD simulations, certain KPIs for the cooling concept are derived. These KPIs are pressure drop, thermal duty and the surface temperature of the hairpins that can be used together with visualization of the flow field. By performing analysis on these parameters the cooling performance of the electric machine can be determined and different geometry designs can be distinguished and analysed. Based on the analysis the difference in cooling performance compared to the current solution can then be determined. By using the conductive heat transfer equation (2.4) in Section 2.2.1 a simplified 2D temperature gradient can be determined. The gradients are calculated for each material between the coolant and heat source. These values are used to illustrate how the temperature difference and cooling performance are affected by the material properties and thicknesses in the path of the heat transfer.

4 Results

In this chapter the result of the development process leading to the final electric machine design and an evaluation of its performance is presented. The steps of determining the improvement area and process development are described in detail followed by creating the geometry of the design in Catia V5. Once a base geometry is created the concept is further analysed by use of CFD simulations and literature to determine the cooling performance of solution and to show the feasibility of the concept. To achieve a realistic concept the focus is then placed on analysing the model and making the concept realizable. To obtain this, consideration of the overall producibility, coolant sealing and electric insulation of the different components in the machine is required. This solution is then evaluated based on a number of KPIs and its results are then validated against a reference solution.

4.1 Identified improvement area

The literature review resulted in determining cooling of the electric machine as the chosen focus area. Improvement in cooling of the electrical machine has the potential of increasing the power density by enabling the use of higher current and thereby higher motor torque during continuous operation. The power density can also be improved by using internal stator cooling which removes the need of an external housing for cooling purposes which can reduce the overall size of the electrical machine. As both the power and size can be individually improved it means that the combined effect may result in a machine with significantly higher power density. This can be utilized to either create a machine of smaller size with the same power or a higher power with the original size. A major part of the heat losses is generated in the copper windings. A more effective cooling of the copper windings result in reduced winding temperatures and thereby reduced copper losses and a higher efficiency. Reducing the heat dissipated from the windings to the surrounding components such as the rotor also reduces its influence on demagnetization in the permanent magnets. When changing to internal stator cooling, the possibility for series production is highly dependent on what solution is used.

4.2 Morphological matrix and generated concepts

The brainstorming session resulted in a large number of concept ideas and sub-solutions to achieve the desired functions. After screening of the various ideas in terms of practicality and functionality the generated concept ideas were determined. These concept ideas from the brainstorming session are then used as input into the morphological matrix as sub-solution options to the sub-functions as shown in Figure 4.1.

	Option 1	Option 2	Option 3	Option 4	Option 5	Option 6	Option 7
Stator slot cooling	Method A	Method B	Method C	Method D	Epoxy resin		
Stator laminate cooling	Solid laminat	Micro channels	Twisted channels	Axial channels	Exterior channels	Rad. channel	Ext. grooves
Housing cooling	Cooling jacket	No ext. stator cooling	Stator contact channel	End winding housing			
Winding	Hairpin	Wire					
End winding cooling	End winding epoxy resin	Fluid jet	Fluid encapsulation				
Intake design	Side inlet	Manifold stator inlets	Channel branching	Fluid reservoir inlets	Nozzles		
Outlet design	Side outlet	Manifold stator outlets	Channel branching	Fluid reservoir outlets	Fluid pan		
Coolant	Dielectric coolant	Water					

Figure 4.1 Morphological matrix (undefined methods due to confidentiality).

From the morphological matrix several cooling concepts are generated and are presented in Figure A.1 in Appendix A. Each of these concepts form a total solution by containing a solution for each corresponding sub-function. All the newly generated concepts are numbered to enable easy tracking in the following determination of the most promising concepts.

4.3 Assessment matrices and concept selection

In Table 4.1 the labelling of the different pre-defined performance criteria are presented to allow for easier visualization in the weighting matrix. The different criteria are labelled from A to J.

Table 4.1 Criteria labelling.

Criteria	Label
Efficiency	A
Continuous power	B
Size	C
Mass producibility	D
Quality	E
Cost	F
Complexity	G
Weight	H
Environmental aspects	I
Structural properties	J

In Figure 4.2 the resulting weighting matrix is shown with corresponding weight values to be used in the following Pugh matrices.

	A	B	C	D	E	F	G	H	I	J	Sum	%	Weight
A		1	1	1	1	1	1	1	1	1	9	20	10
B	0		0,5	1	1	1	1	1	1	1	7,5	16,7	8
C	0	0,5		1	1	1	1	1	1	1	7,5	16,7	8
D	0	0	0		1	1	1	1	1	1	6	13,3	7
E	0	0	0	0		1	1	1	1	1	5	11,1	6
F	0	0	0	0	0		1	1	1	1	4	8,9	5
G	0	0	0	0	0	0		1	0	0,5	1,5	3,3	3
H	0	0	0	0	0	0	0		0	0,5	0,5	1,1	1
I	0	0	0	0	0	0	1	1		1	3	6,7	4
J	0	0	0	0	0	0	0,5	0,5	0		1	2,2	2
											45		

Figure 4.2 Weighting matrix.

In Figure B.1 in Appendix B the resulting Pugh matrix with all the generated concepts, criteria and weighting levels is shown. The criteria are ordered on criteria labelling order, see Table 4.1, with A at the top and J at the bottom. Furthermore the concepts are listed as numbers corresponding to the concept numbering in Figure A.1 in Appendix A. In this matrix the current solution was used as the reference against which all the other concepts are compared. It can be seen that most of the generated concepts that recieved a positive score provide benefits when compared to the current solution.

This means that the three concepts which received a negative score can be removed from further analysis and thereby narrowing down the number of concepts.

From the first iteration of the weighted Pugh matrix it is seen that all the remaining concepts have advantages compared to the current solution and therefore a new reference needs to be determined for the next iteration. Concept 1 is chosen as the reference to be used for comparison with the other concepts in the second weighted Pugh matrix, shown in Figure B.2 in Appendix B, since it is considered to be the most promising concept. Based on the literature study of losses in the electrical machine, as described in Section 2.1.5, this concept is considered to have the best potential in improving efficiency and continuous power which are two of the highest prioritized design criteria.

From the Pugh matrix in Figure B.2 in Appendix B there are six concepts that show total scores which are equal to or above -10 which is used as the cut-off point. The chosen concepts to proceed with are marked as green in the matrix. The current solution is still present in the matrix to only be used as a comparison tool to visualize concepts that achieve a low score.

4.3.1 Description of the chosen concept types

In this section the six chosen concept types from the Pugh matrix analysis are described in more detail for utilization in concept evaluation with technical experts. As several of the concepts are either very similar to one another or a combination of two solutions these are described together in the following sections.

4.3.1.1 Internal and end region cooling – concepts 1, 5 and 11

Concept 1 is constructed with internal cooling and fluid encapsulated end regions. The coolant travels from one end region to the other. A hairpin design is used rather than traditional wire winding to improve the fill factor which can allow for more efficient usage of the available space inside the stator slots as well as possibly reducing the axial length of the machine. The choice in cooling fluid for this concept is highly dependent on the ability of insulating the coolant from both the stator core as well as the hairpins. By using a dielectric fluid such as oil minimum insulation is required due to its dielectric properties. However if a non-dielectric fluid, such as water, is to be used, proper insulation is a requirement to avoid short circuit.

There are two additional more complex similar concepts, 5 and 11, which shows promise as can be seen in the Pugh matrix if additional cooling is required. These alternative concepts are in the form of solution combinations with added internal stator channels. The more promising of the two, concept 11, uses internal axial cooling channels through the stator core to provide additional cooling performance. Concept 5 has added micro channels through the stator lamination which increases the cooled surface but it also increases the complexity of the design. The influence on the magnetic flux field based on the position of the channels do however need to be considered. Having the additional channels through the stator lamination also adds difficulty with regards to sealing and possibly electrical insulation depending on the type of fluid.

4.3.1.2 Axial stator channels – concepts 6 and 7

In order to avoid coolant being in contact or risk getting in contact with the copper, cooling channels inside the stator core can be used to extract heat from the machine. The stator channels can be optimized with regards to size, positioning, number of channels, routing etc. Concept 7 has straight axial channels going straight through the stator core while the channels in concept 6 has helical shapes. Helical shaped channels increases the surface area but also increase the complexity in terms of manufacturing, sealing and electrical insulation. The coolant will be pumped in from one side of the stator and led through to the other side. In order to reduce the amount of inlets and outlets to the stator lamination stack, the channels in the stator can branch out directly after the inlet and unite before exiting the stator core outlet. This provides cooling to the core as well as cooling closer to the copper compared to a conventional cooling jacket solution. Care must be taken to not negatively influence the magnetic flux. Three different example positions of the internal stator cooling channels which were investigated are shown in Figure 4.3.

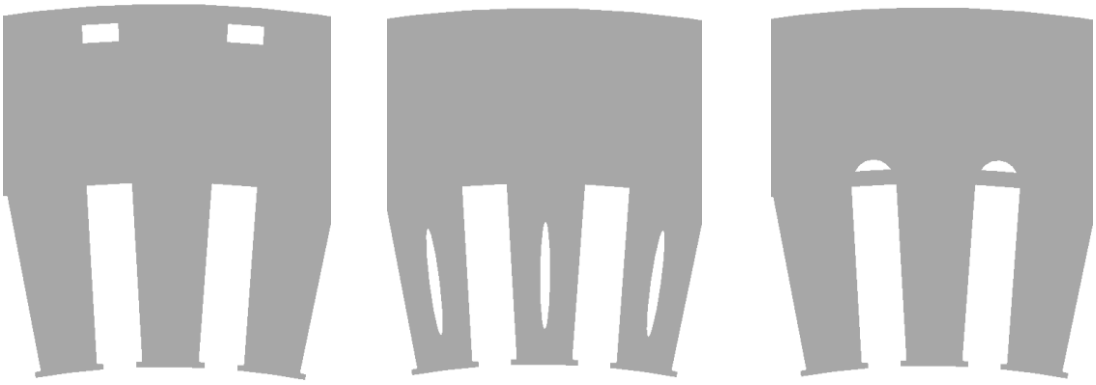

(a) Outer rim *(b) In teeth* *(c) Above slots*

Figure 4.3 Three different positions of internal stator cooling channels.

4.3.1.3 External stator cooling – concept 8

This concept resembles the conventional cooling jacket solution. The main difference is that instead of having an inner and outer housing, only one housing is used that directly contacts the stator core as shown in Figure 4.4. The inner wall of the housing has a spiral shaped cooling channel geometry, directing the coolant flowing between the housing and the outside of the stator. This allows for a more direct cooling of the heat source, providing more efficient cooling. One advantage of this solution is that the existing machine does not have to change much. The downside of this concept is that it still cools the machine on the outside of the stator core and not as close to one of the major heat sources, the copper windings. The solution is further improved by incorporating hairpins to improve the fill rate in the stator slot.

Figure 4.4 Cooling jacket in direct contact with stator.

4.3.2 Evaluation with experts

By having a discussion with technical experts within the field of electrical machines three of the concept areas were disregarded. The concepts which have cooling through internal stator channels are disregarded as this is considered to potentially have a significant negative effect on the magnetic flux. If the cooling channels are placed in the teeth the negative effects are increased due to magnetic saturation. This means that in order to utilize internal cooling channels they would need to be placed towards the rim of an extended stator core to avoid any magnetic field obstruction. However by placing the channels at a distance further away from the stator slots the main benefit of using internal cooling channels is lost and therefore concepts 5, 6, 7 and 11 are disregarded. There is however still an option of using it as a further elaboration of the chosen concepts if additional cooling is required but it will not be considered as a main cooling solution. Concept 8 is quite similar to the current cooling jacket solution but it removes the need for an inner housing and has coolant in direct connection to the stator core. Cooling of the stator core outer rim is therefore better compared to the conventional solution, however the main heat sources are not efficiently cooled. There are also issues which may appear when using this solution such as coolant insulation and the space between the stator laminations which needs to be sealed together to avoid leakage that can result in machine failure due to short circuit. Due to these problems this concept is not chosen for further development.

Based on the input from the technical experts, concept 1 is chosen due to its high potential. Having coolant in direct contact with main heat sources allows for an effective convective heat transfer. Using a water/glycol mix as coolant has the highest potential in terms of both heat transfer capabilities and being able to use the existing cooling system. It does however not come without issues and coming up with a reliable solution for insulating the coolant from the components is the main concern.

4.4 Concept design

A representative CAD model of the electrical machine was created by using existing reference models or based on design specifications. A combination of collaboration with technical experts and CAE engineers, in the fields of electrical drive and cooling system, as well as a literature study based on scientific articles, patents and competitor analysis was used for designing the more innovative parts. These references allowed for the creation of a machine with realistic design parameters so that accurate CFD calculations of the cooling performance could be performed. Some of the components which are created in-house from scratch without any exact parameter values will however require further testing to verify that their design does not influence the machine in a negative way. As the purpose is to perform CFD calculations of the cooling performance, the design of the axle and the interior of the rotor and stator cores are disregarded and made as a solid parts for illustration purposes only. By not performing significant changes to the rotor and stator design, the electromagnetic performance of the machine can be considered as unchanged. Figure 4.5 shows an external view of the complete PMSM design with wires for the three-phase connection as well as cooling inlet and outlet interfaces. Each component will hereafter be described.

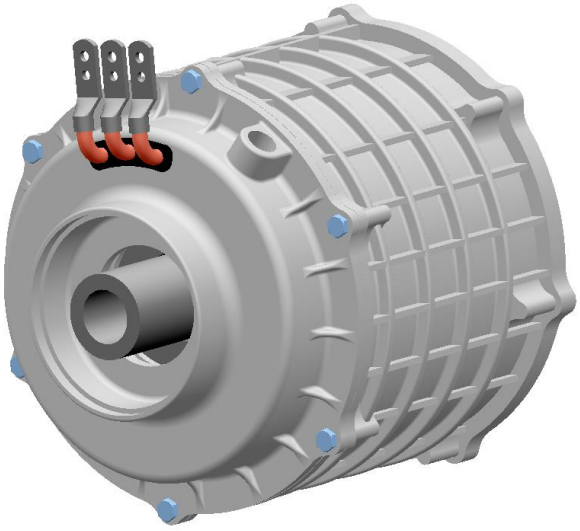

Figure 4.5 Complete PMSM design.

To produce an easier visualization of the machine components, while retaining their relative position to one another, an exploded-view of the main components in the axial direction is shown in Figure 4.6. The figure shows how the components inside the housing are positioned relative to one another. It also illustrates how the welded hairpin end region is connected to the three-phase connector, shown as a black circular component with orange high voltage cables.

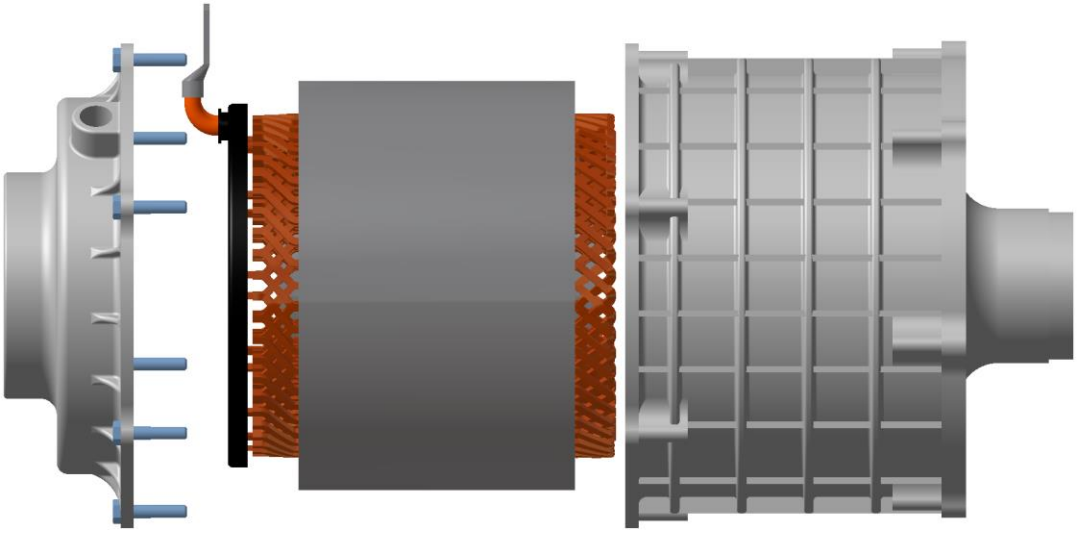

Figure 4.6 Exploded-view of the PMSM design.

The housing of the electric machine is typically used both to provide a cooling solution in the form of a cooling jacket between two housing surfaces as well as serving as a protective casing. However by removing the need for a cooling jacket in this design there is no longer any need for two external overlapping housings. The design of the housing is therefore separated into a main housing and a housing lid.

The housing is designed to closely resemble a reference design so that it can, in terms of structural properties, provide comparable results. The location of the coolant inlet on the housing is designed such that it resembles the current cooling jacket inlet location for reduced packability complexity.

To enclose the electric machine a lid is designed for attachment on the three phase connection side of the stator. The location of the coolant outlet on the housing lid is designed such that it resembles the current cooling jacket outlet location for reduced packability complexity. The two housing components are made in aluminium through casting and machining in the same way as conventional housings. The fluid is led into the inlet in the housing and enters into the first fluid chamber. Here it cools the end regions of the conductors in the stator. It then flows through the entire length of the stator. Thereafter the coolant enters the second chamber and provides cooling for the end regions on the other side of the stator. It then passes through the outlet of the housing lid.

Instead of using traditional copper windings a hairpin solution, as shown in Figure 4.7, is created. This is done to achieve a higher fill rate, by having a rectangular cross section, and a reduced end region size. The hairpins are on one end twisted and bent to obtain a continuous conductor which can be inserted into the stator slot. Thereafter the straight ends are bent and joint together with either another hairpin or to the 3-phase connector. Twelve of the hairpins are extended to serve as connections, two per phase for each hairpin row.

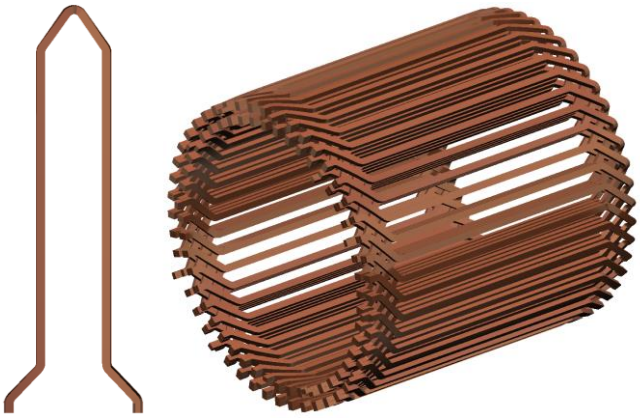

Figure 4.7 Single hairpin and the full hairpin assembly.

Figure 4.8 shows how the hairpins are connected to the three phase power cables using a connection ring. The three phases are then connected to the inverter. The ring is mounted on the hairpins and makes contact with 12 hairpin ends. The rear face of the ring has 12 connection points distributed symmetrically with 30 degrees of separation. The three phase cables are routed through a dedicated hole in the housing lid which is then sealed in order to prevent leakage of coolant. This connecting ring solution is not designed in detail during this cooling concept study but is rather made to be representative in terms of dimensions in order to achieve a realistic CFD analysis.

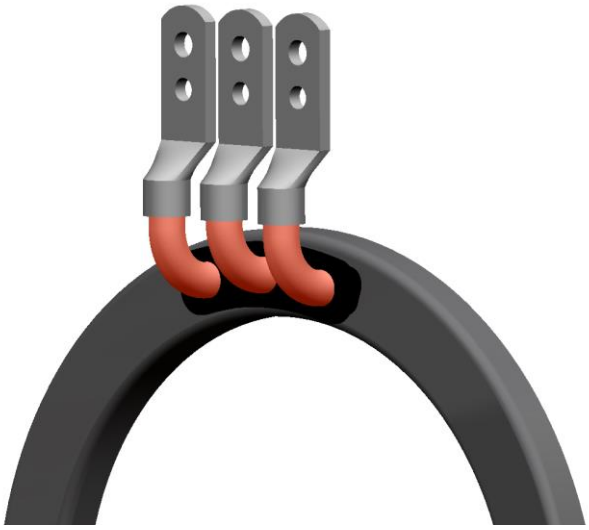

Figure 4.8 3 phase cable connection.

4.5 CFD

In the following sections validation of the simulations followed by the results of the CFD analysis are presented. Figure 4.9 below is used to further show the design of the fluid-occupied volume inside the base design with arrows indicating inlet and outlet flow directions.

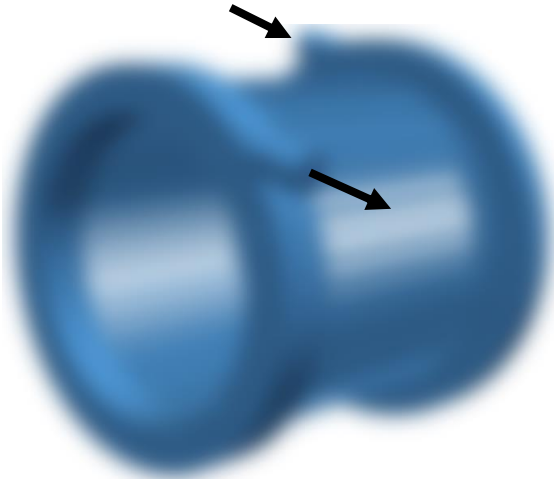

Figure 4.9 Fluid-occupied volume inside the casing with arrows representing inlet and outlet flow direction (blurred due to confidentiality).

4.5.1 Validation of the simulation results

Determination of the CFD simulations accuracy is important to validate the simulated results. By analysing Figure 4.10 it can be seen that the residuals during the simulation shows an iterative convergence.

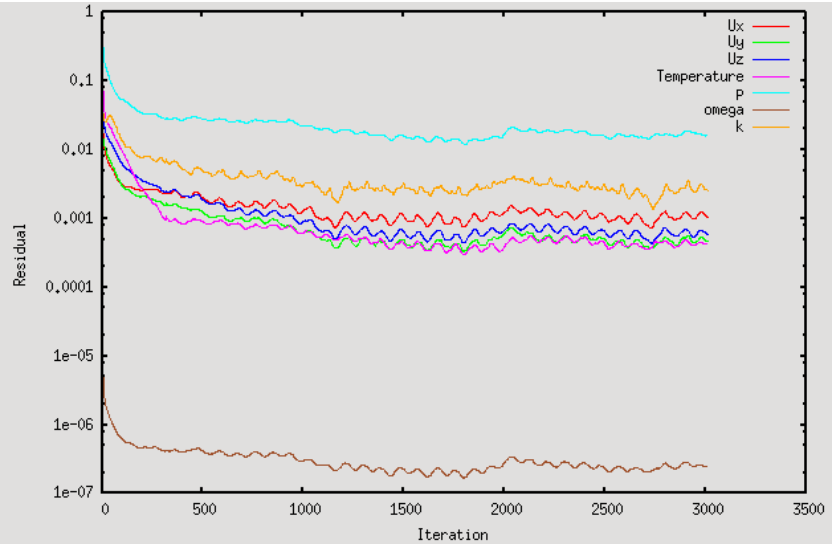

Figure 4.10 Residual plot of the base design simulation.

As all simulations are set up with a constant heat effect, volumetric flow rate and the same coolant properties it allows for analytical calculations of the temperature difference. The temperature difference between the inlet and outlet is calculated according to equation (3.2) in Section 3.3.1 and shown in equation (4.1) below. The outlet temperature can then be calculated according to equation (4.2).

$$\Delta T_{analytical} = \frac{3000}{\left(1069 \cdot 3340 \cdot \frac{8}{60 \cdot 10^3}\right)} = 6.302\ K \tag{4.1}$$

$$T_{out_{analytical}} = T_{in} + \Delta T_{analytical} = 349.302\ K \tag{4.2}$$

The analytically calculated temperature difference value is then used to verify the simulation results by comparison to the simulated temperature difference. The difference between the simulated and the analytically calculated values is between 0.08 - 0.2 % which validates the results. These values are taken from the last iteration and due to the residuals fluctuation, seen in Figure 4.10, a mean value of the last few iterations would have most likely improved the accuracy. The patch integrated volumetric flow rate through the outlet is also controlled and verified that it is equal to that of the inlet.

The dimensionless wall distance y^+ is used to validate how applicable the used wall function is. In Figure 4.11 the y^+ values on the hairpin surfaces are shown. The y^+ values on the hairpins have a minimum of 0.0024, maximum of 9.6497 and the average y^+ over the surface is 2.1978. Menter, et al. (2003) determined that having $y^+ < 2$ is not necessary for complex flows that are used in an industrial setting and as such the average y^+ from the simulation results are deemed sufficiently low.

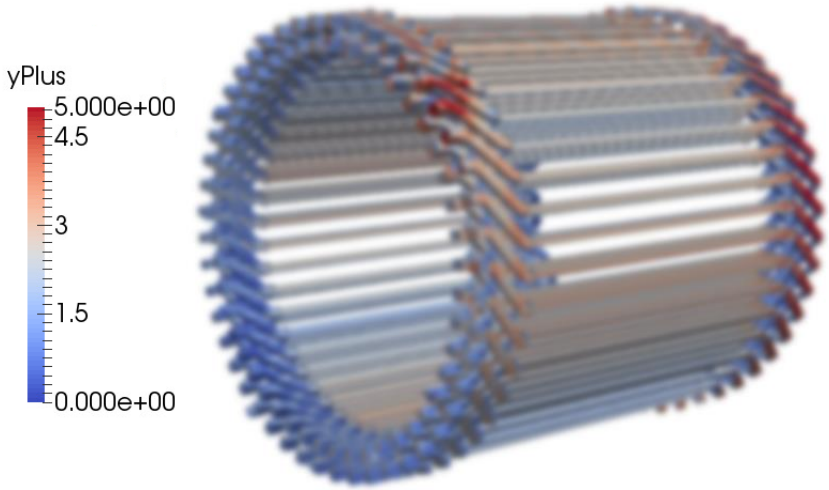

Figure 4.11 Value of y^+ on the hairpins (blurred due to confidentiality).

4.5.2 Base design

The initial model created is used as reference design for comparison to designs with changed geometries in the CFD simulations. The model has inlet and outlet angled in similar fashion as that of the current cooling jacket design. The hydraulic diameter was calculated to determine the Reynolds number which was approximately 500. The flow is determined to be laminar as the Reynolds number is significantly lower than 2300 and based on the form of the equations, small adjustments in hydraulic diameter will not change this.

The temperature distribution of the hairpins in the base design is shown in Figure 4.12 below. However in this model the hairpins are not simulated with thermal conduction inside the hairpin volume which influence the uneven distribution. By performing additional simulations with thermal conduction in the hairpins and copper as the conductor material the temperature distribution should be closer in relation to the average surface temperature used for comparison. Having large differences in temperature between the separate parts of the components results in thermal stresses that can lead to fractures in the insulating materials. The temperature difference of the hairpins between the inlet and outlet sides is approximately 17 °C which is significantly lower than what commonly occurs in conventionally cooled machines. This is shown by Grunditz (2016) where the temperature difference between the end regions and the windings in the slots is determined to be approximately 25 °C. The temperatures shown on the hairpins in Figure 4.12 is well below the limits of commonly used insulations. The insulation can typically withstand temperatures around 180 °C with slight variations between different materials (Temco, 2017).

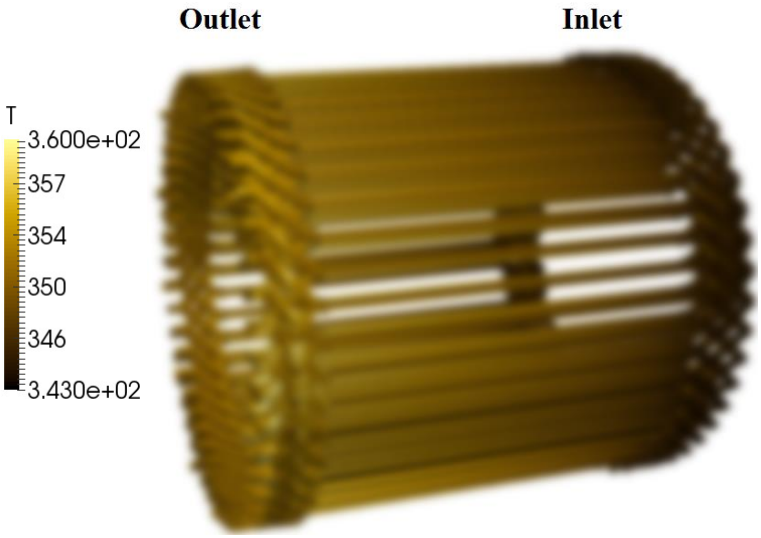

Figure 4.12 Hairpin surface temperature at 3000 W effect with 70 °C coolant inlet temperature and 8 L/min volumetric flow rate (blurred due to confidentiality).

In Figure 4.13 below the temperature distribution and the velocity flow fields at the inlet position in the YZ-plane are shown. The velocity field shows that the positioning of the inlet creates a flow that follows the housing wall in a circular fashion which contributes to the equalization in flow around the hairpin end regions. It can however clearly be seen that there is still a large significant difference in flow velocity in the fluid domain. The figure also shows an even temperature distribution in the fluid volume at the inlet side which is approximately the inlet temperature. The same range has been used for both the temperature and velocity scales for all designs which allows for clearer visual comparisons to be made. Different colour scales has been used for the temperature and velocity in order to make an easier distinction between the various sections of the flow field and have been chosen according to VCC standards.

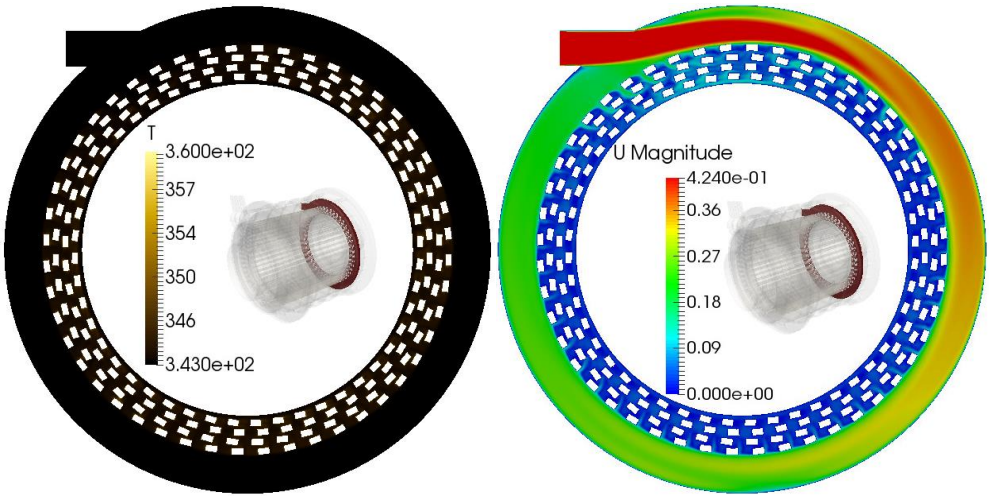

(a) Temperature distribution [K] *(b) Flow velocity magnitude [m/s]*

Figure 4.13 Temperature, (a), and velocity, (b), for the base design in the YZ-plane at centre of the inlet.

The inequality in the flow velocity in the fluid reservoirs is further demonstrated in Figure 4.14 where the temperature distribution and the velocity flow fields at the outlet position are shown. It can be seen that the velocity increases closer to the outlet which results in increased temperatures at the opposite side. A recirculation zone with low velocities can also be seen in the outlet.

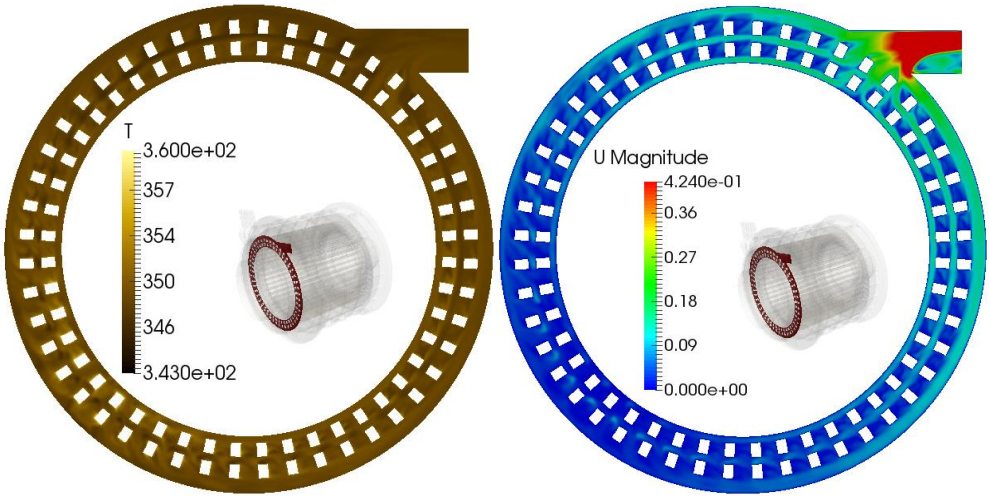

(a) Temperature distribution [K] *(b) Flow velocity magnitude [m/s]*

Figure 4.14 Temperature, (a), and velocity, (b), for the base design in the YZ-plane at centre of the outlet.

From the simulation results the Nusselt number is calculated as 8.47 which shows that the heat transfer in the concept design is mostly convection dominated.

4.5.3 Changed inlet design

A changed inlet design was created and analysed with the intention of achieving a more uniform bidirectional flow field. This design did however enhance the inequality of the flow to the point of stagnation on the opposite side as can be seen in Figure 4.15.

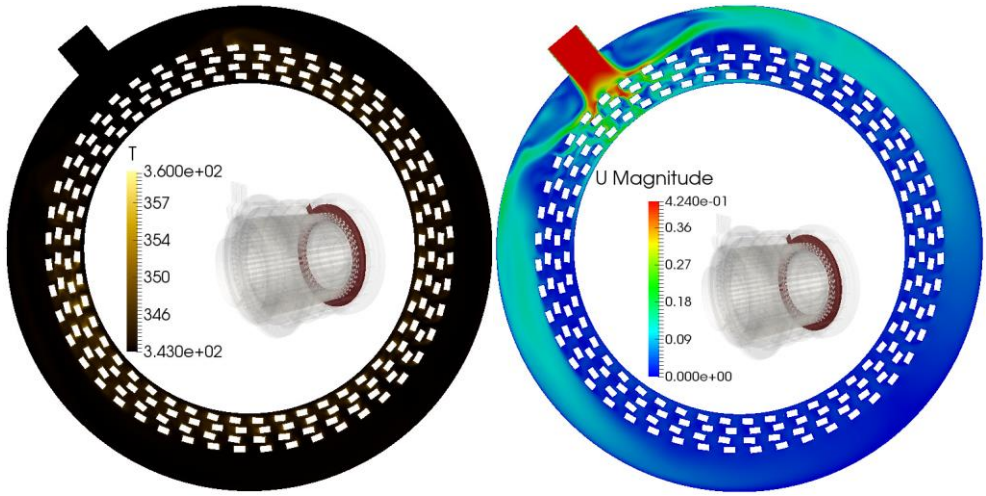

(a) Temperature distribution [K] *(b) Flow velocity magnitude [m/s]*

Figure 4.15 Temperature, (a), and velocity, (b), for the changed inlet design in the YZ-plane at centre of the inlet.

The post processed values of the KPIs for the changed inlet design are normalized against the base design and presented in Table 4.2 below. The changes resulted in an increased hairpin surface temperature and a reduction of the thermal duty. There was however no significant difference in pressure drop between the two designs.

Table 4.2 KPI for the changed inlet design normalized against base design.

Normalized key performance indicators	Change
Wetted heat emitting surface area $[m^2]$	0 %
Average hairpin surface temperature $[K]$	+0.07 %
Convective heat transfer coefficient $[W/m^2K]$	-6.64 %
Thermal duty $[W/K]$	-6.73 %
Pressure drop $[Pa]$	-0.84 %

4.5.4 Radial outlet design

From the base design it could be seen in Figure 4.14 that there is a recirculation zone present in the outlet which influence the designs pressure drop. Figure 4.16 shows the generation of turbulence at this location.

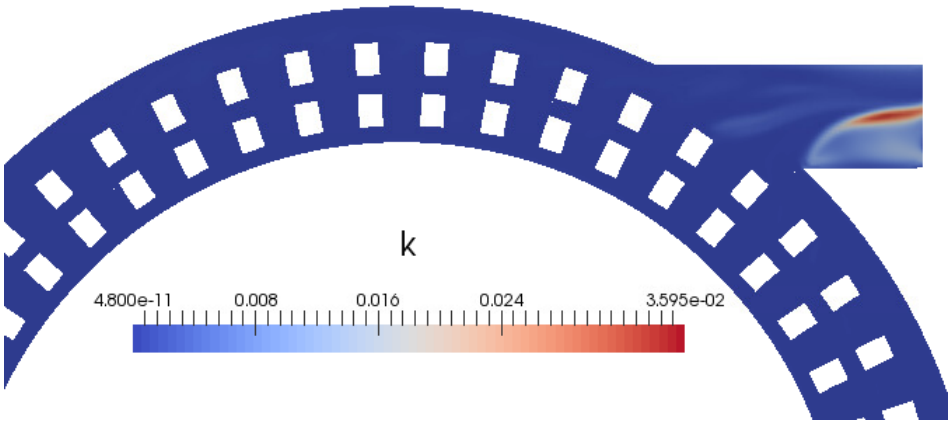

Figure 4.16 Turbulence generation in YZ-plane at centre of the outlet.

To reduce this recirculation zone a changed outlet design was created and analysed. In Figure 4.17 below the temperature and velocity flow fields at the outlet position of the new design is shown. This figure shows a more uniform flow through the outlet with reduced recirculation zones.

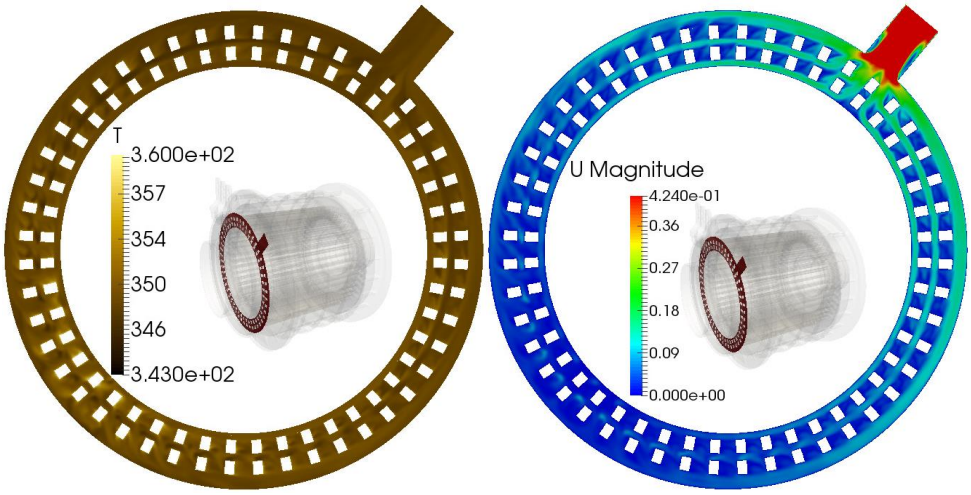

(a) Temperature distribution [K] *(b) Flow velocity magnitude [m/s]*

Figure 4.17 Temperature, (a), and velocity, (b), for the radial outlet design in the YZ-plane at centre of the outlet.

The benefit of changing the outlet design is shown in Table 4.3 where the pressure drop is reduced. The changes do not negatively influence the convective heat transfer compared to the base design as can be seen from the similar values in thermal duty and hairpin surface temperature.

Table 4.3 KPI for the radial outlet design normalized against base design.

Normalized key performance indicators	Change
Wetted heat emitting surface area $[m^2]$	0 %
Average hairpin surface temperature $[K]$	+0.01 %
Convective heat transfer coefficient $[W/m^2K]$	-0.15 %
Thermal duty $[W/K]$	-0.13 %
Pressure drop $[Pa]$	-3.58 %

4.5.5 Changed channel geometry

In order to improve the convective heat transfer a design with a larger wetted heat emitting surface area was created and analysed. The overall cross-sectional channel area was kept the same. The design showed an 11 % increase in pressure drop, as seen in Table 4.4, which may be caused by increased friction as a consequence of the larger surface area. It can be seen that change in channel design resulted in the desired improvements in thermal convection as the thermal duty was increased by approximately 19 %.

Table 4.4 KPI for the changed channel geometry design normalized against base design.

Normalized key performance indicators	Change
Wetted heat emitting surface area $[m^2]$	+11.24 %
Average hairpin surface temperature $[K]$	-0.19 %
Convective heat transfer coefficient $[W/m^2K]$	+7.09 %
Thermal duty $[W/K]$	+19.13 %
Pressure drop $[Pa]$	+10.95 %

A typical conventional cooling jacket has a pressure drop that is approximately 8 times higher than the base design which means that the increase of approximately 11 % in the changed channel design still constitutes as a decrease in total pressure drop of the cooling system.

4.5.6 Final CFD concept solution

By analysing the generated design concepts it can be seen that a combination of the radial outlet design and the changed channel design should show to be an improvement over the base design with regards to all KPIs. In the Figures 4.20 - 4.21 the flow fields and temperature distribution of the final design are shown.

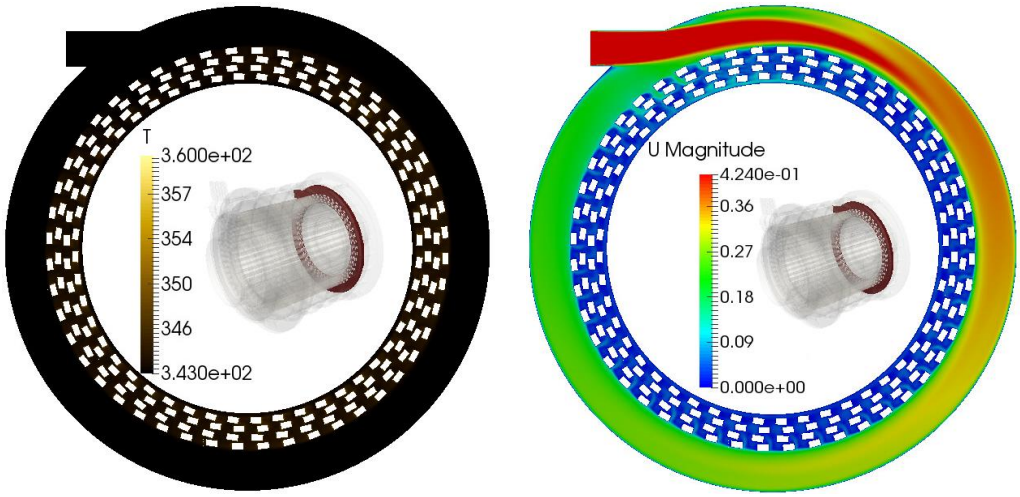

(a) Temperature distribution [K] *(b) Flow velocity magnitude [m/s]*

Figure 4.18 Temperature, (a), and velocity, (b), for the final design in the YZ-plane at centre of the inlet.

By changing the outlet design, as seen in Figure 4.19 below, a more uniform flow is achieved in the outlet compared to the base design. Having a changed channel design did however influence the flow which is shown as a larger recirculation zone on one side.

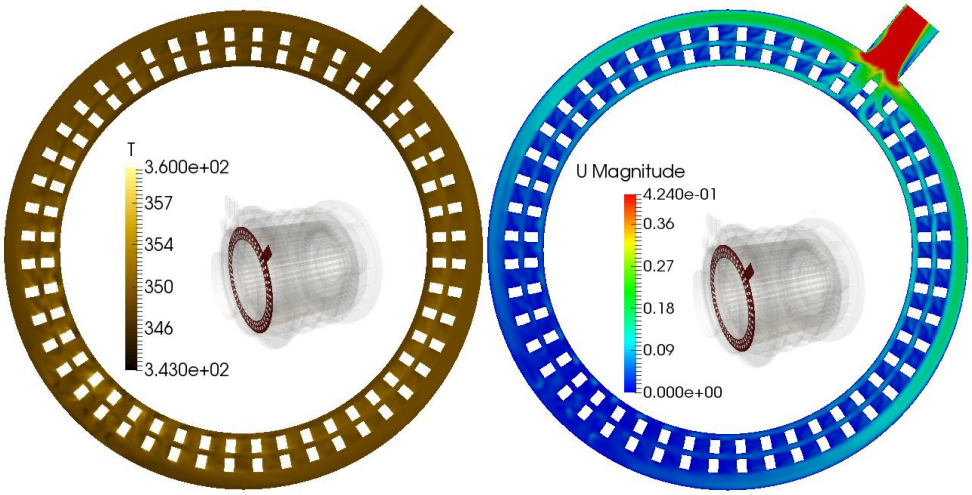

(a) Temperature distribution [K] *(b) Flow velocity magnitude [m/s]*

Figure 4.19 Temperature, (a), and velocity, (b), for the final design in the YZ-plane at centre of the outlet.

Combining the two designs which showed the best values generated a better design, as seen in Table 4.5. The solution has the same 19 % improvement in thermal duty as the changed channel design and despite the increased surface area the pressure drop was reduced by approximately 2 % over the base design and only slightly higher than the radial outlet design. This design combination is therefore chosen as the final design concept since it resulted in the best combination of high thermal duty and low pressure drop.

Table 4.5 KPI for the final CFD design normalized against base design.

Normalized key performance indicators	Change
Wetted heat emitting surface area $[m^2]$	+11.24 %
Average hairpin surface temperature $[K]$	-0.19 %
Convective heat transfer coefficient $[W/m^2K]$	+7.02 %
Thermal duty $[W/K]$	+19.00 %
Pressure drop $[Pa]$	-2.32 %

4.5.7 Conjugate heat transfer simulation

Performing a CHT simulation on the base design showed temperature distributions in the inlet and outlet chambers according to Figure 4.20. The outlet temperature should be the same for all cases as estimated by the numerical analytical calculation, however the temperature difference seen in the simulation is significantly lower. This is because of the simulations are not yet converged as the simulation has not run its full number of iterations. This is due to limitations in resource allocation and an update in boundary conditions. The results shown in Figure 4.20 are interim results after 4000 iterations and even though the results are not usable they show that the principle is sound, the setup is functional and that the simulation does not diverge.

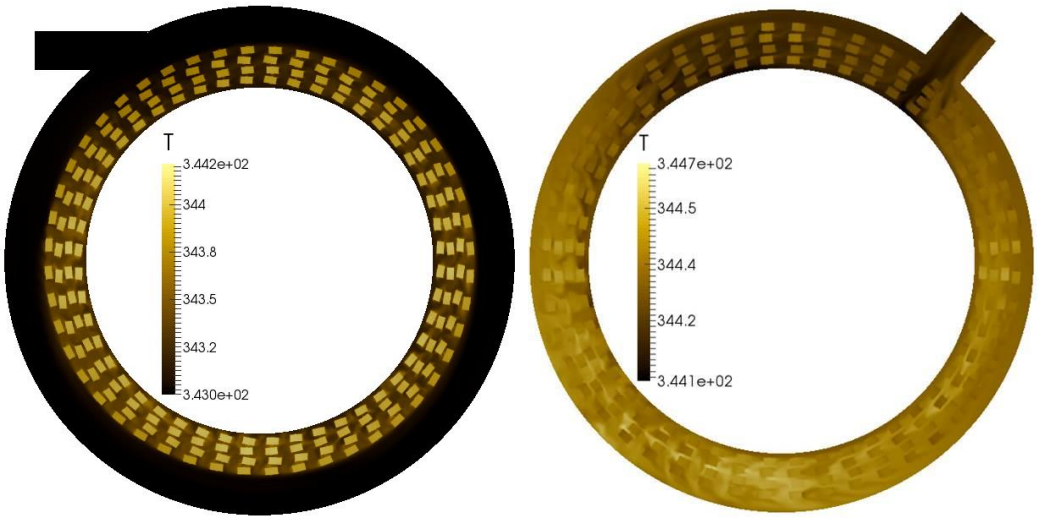

(a) Inlet temperature distribution [K] *(b) Outlet temperature distribution [K]*

Figure 4.20 Temperature distribution in the inlet chamber (a) and outlet chamber (b) for the CHT simulation interim results.

4.6 Hairpin insulation

Without proper insulation, the electrical conductive properties of the water/glycol coolant can result in failure of the machine due to short-circuit. The hairpins therefore require an insulating layer. The eddy currents induced into all parts that are exposed to the coolant also needs to be insulated from the conductive fluid. The insulation needs to be durable as it has to maintain its dielectric properties and remain waterproof over the entire lifecycle of the machine. One important aspect to consider is to have similar thermal expansion of the conductor and insulating material to avoid high thermal stresses in the material. These stresses can lead to fracture in the insulation layer.

Having an insulating layer on the hairpins takes up valuable space inside the slots which has a negative effect on the copper fill rate. In order to maximise the usable space in the slot, the insulation should be kept as thin as possible. A thick insulation layer also has a negative effect on heat transfer. The required thickness of the insulation is based on for example the material properties, applied voltage, dimensions of the conductor and what coolant is used. The dielectric constant of the fluid can be reduced by using a glycol with a lower electrical conductivity, thus decreasing the required amount of insulation. The technique of having insulating coatings on conductors in contact with water is widely used when it comes to submersible electric motors. The approach has been used in the industry for a long time and is mass producible for copper windings. The same principle should be applicable to the hairpin conductors ensuring proper electric insulation for the machine. Having an insulation thickness of approximately 0.25 mm has been estimated as appropriate for the developed concept (Emgee, n.d.).

4.7 Sealing

In order for the cooling concept to function, the entire fluid volume requires a watertight sealing. Where the separate components that form the boundaries for the fluid meet, an interface exists that needs sealing. Any leaks could cause damage to the machine which is not acceptable. The sealing must also last the entire lifespan of the vehicle since

service of the electric machine would be very costly due to its inaccessibility. A thorough investigation of all interfaces between the different components has been performed and appropriate sealing techniques has been determined.

4.8 Evaluation and validation

In the following section the internal cooling design is evaluated and its performance is validated against a conventional cooling jacket reference design. The design criteria used are efficiency, power, size & packability, mass producibility and cooling performance.

4.8.1 Efficiency & Power

Many types of internal cooling solutions have been investigated but few can be found used in the industry. Internal cooling methods have been shown to improve the performance of the machine with regards to efficiency and continuous power output. Two main aspects when it comes to efficiency and continuous power is to reduce the temperature in the copper hairpins to reduce electrical resistance in the copper as well as maintaining a magnet temperature to avoid demagnetization which reduces the maximum continuous power. Losses in the stator and rotor cores however are reduced with increased temperatures so by having a more local cooling closer to the temperature sensitive components such as the hairpins and magnets losses in the stator can be reduced. The current cooling jacket solution primarily cools the stator core and indirectly the hairpins by heat conduction through the stator laminates. This means that the temperature in the stator is reduced with increasing radial distance and as such the iron losses in the stator core are increased and cooling effect on the windings is lower which results in increased copper losses.

When comparing an internal cooling concept using oil to the conventional cooling jacket with a water/glycol coolant for a switched reluctance machine, the total losses of the machine was reduced by 12 % for a specific operating point and continuous torque output was increased by 300 % (Liu, et al., 2015). In a study performed by Schiefer & Doppelbauer (2015) which compares the cooling jacket to another version of internal cooling, the temperatures of the end region, effective winding and teeth were significantly reduced. These patterns and trends are also shown in a study by Lindh, et al. (2017). In this study the cooling simulations were also validated against experimental data which showed comparable results. The analysis also showed that the current density in the windings could be increased with the direct winding cooling method.

Since the cooling method directly influence the heat dissipation of several temperature critical components, this allows actively control the volumetric flow rate. This can allow for active control of the cooling effect based on the machines torque and rotational speed. This control method can be utilized for efficiency optimization.

4.8.2 Size & Packability

The overall dimensions of the machine with the new cooling geometry has also been compared to that of the reference machine. The outer diameter as well as the length of the two machine designs can be seen in Table 4.6. The values for the reference design are approximations to not disclose confidential information.

Table 4.6 Outer dimensions of the conventionally cooled machine and new concept.

	Conventional external cooling	Internal cooling design
Diameter [mm]	280	258.0
Length [mm]	290	264.6

The new cooling design manages to reduce the outer diameter of the machine by 22 mm since the housing no longer needs to be made in two layers with cooling channels. This is a reduction by approximately 7.9 %. The length reduction is 25.4 mm, largely due to the change from conventional windings in the slots to a more compact hairpin solution. This is a length reduction of approximately 8.8 %. It can be determined that the packability is improved since the new design reduces the overall size of the electric machine. It also keeps the shape similar to that of the original without any bulky features. By removing the additional outer housing the aluminium weight is reduced by approximately 1.5 kg. The change in length and diameter between the developed concept and the reference is shown in Figure 4.21.

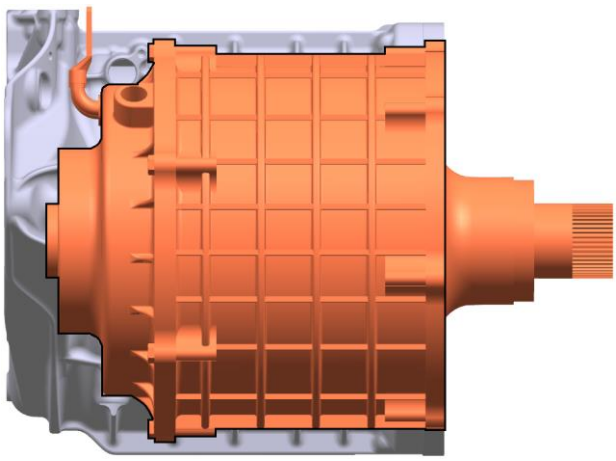

Figure 4.21 Size comparison between the developed concept (orange) and reference machine (grey).

4.8.3 Mass producibility

Compared to the assembly process of the cooling jacket the assembly order is slightly changed and has a few added steps. The added steps in the assembly process are formed by an increased number of components and a slightly different assembly process. Each of the individual assembly processes required for this concept are well-suited for mass production. For these reasons the developed concept is deemed to be suitable for mass production.

4.8.4 Cooling performance

The two designs are compared with approximately the same heat flow, volumetric flow rate and coolant inlet temperature. The convective heat transfer coefficient of the current cooling jacket design is about 80 % higher compared to the final design. However the wetted surface area of the cooling jacket is only a third of the final design which means that the thermal duty is roughly twice as high as the cooling jacket design.

This means that the machine is more efficiently cooled and the wall temperature is closer to that of the coolant. From the final design CFD results it is determined that the pressure drop for the final design is approximately a factor 7-8 lower than that of a representative cooling jacket solution.

The next step in the evaluation of the cooling performance is to investigate the path of the heat flow. The thermal conductivity of the different materials that transfer the heat from the conductors to the water can be seen in Table 4.7. In order to estimate the behaviour of the resin impregnated windings of the reference solution, they are treated like a single material with an equivalent thermal conductivity according to Popescu, et al. (2013).

Table 4.7 Thermal conductivities, k, for relevant materials. (Andersson, 2013) (Popescu, et al., 2013) (Böckh & Wetzel, 2012)

Material	Thermal conductivity $[W/mK]$
Copper	392
Electrical steel, in plane of lamination	28
Insulation	0.2
Aluminium	240
Resin/copper equivalent	0.6

The surface areas used in determining the temperature gradients are presented in Table 4.8 below. They are determined from either the wetted surface areas or an estimation based on the CAD design.

Table 4.8 Transition surface areas.

Transition surface	Approximate surface areas $[m^2]$
Cooling jacket – Coolant to Inner housing	0.22
Cooling jacket – Inner housing to stator core	0.13
Cooling jacket – Stator core to stator slot	0.34

For the cooling jacket the heat needs to travel through several components in order to reach the coolant, see Figure 4.22. For the internal cooling design the path is shorter and made up of fewer components. The shape of the gradient between the coolant and the wall is only for illustrative purposes and does not portray the real gradient. This does therefore not accurately convey the exact values for the cooling jacket but rather shows the principle of the cooling design.

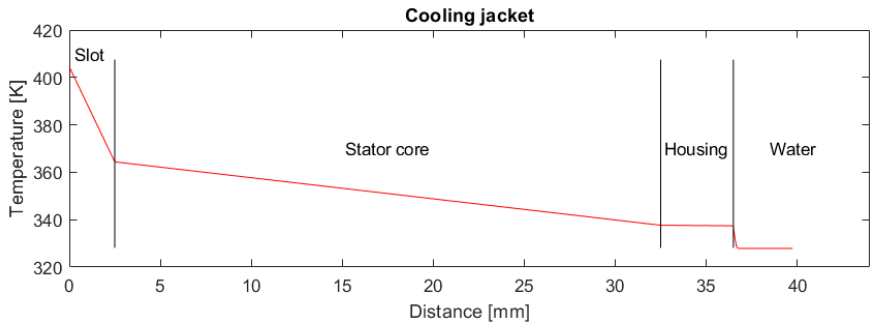

Figure 4.22 Heat transfer gradient for the cooling jacket.

The temperature difference between the windings and the coolant for the cooling jacket is approximately 76 °C. The resulting temperatures in the cooling jacket design are in line with what is shown by Grunditz (2016) for a similar case with approximately the same amount of heat generation. By using the same procedure for the internal cooling design this difference is instead reduced to 6 °C, which is a reduction of about 92 %. This is due to the reduced distance through which the heat needs to travel. The distance is reduced in the internal cooling design by roughly 95 %.

5 Discussion

The CFD simulations performed in this study are based on a number of assumptions and simplifications. Radiation is ignored although it as always present to some extent. Another aspect that could give rise to errors in the result is that a heat flux load is not applied to all heat emitting components in contact with the coolant, which would have increased the wetted surface area and thereby also the thermal duty. Yet another simplification is that a uniform heat flux is assumed on all heat generating surfaces. Furthermore adiabatic conditions are assumed which means that the heat can only be transferred away from the machine through the outlet and not through the casing of the machine or through the axle. These assumptions have been made as they have simplified the simulations and because they have been deemed to not affect the results to a large extent. All of these assumption do however build errors into the results to some degree. That means that the absolute values of cooling performance presented should be regarded with these simplifications kept in mind. The results from this setup should roughly correspond to the actual values and still allow for a fair comparison when investigating the difference in cooling performance between the geometries. The CFD simulations in this study are meant to show the potential of the developed cooling solution, not the absolute performance with high precision.

The reduced pressure drop seen in the simulations is likely due to the relatively low flow velocities through the machine. Another aspect that has a positive influence on the pressure drop is the fact that the flow behaviour through the machine is relatively unidirectional. The significantly reduced pressure drop means that less energy will be needed to pump the fluid through the machine. Alternatively a more aggressive cooling geometry can be created that improves the cooling performance even more since the increased pressure drop should still be lower than for the cooling jacket.

A CHT model of the final design was set up in this study but was not fully completed. The case was not possible to run in parallel on the VCC high performance computing resources which meant that the case was run locally. The computations also needed significantly more iterations to converge compared to the previous simulations. After 6000 iterations, the outlet temperature had increased by around 2 degrees which indicates that only about a third of the applied heat load has been transferred to the coolant. Provided that the issue regarding running the simulation in parallel is solved, the setup should be able to provide the desired results given enough iterations. This would also allow for more KPIs to be determined such as the internal temperature distribution in the copper.

An increase in overall efficiency due to lower copper losses and reduced pumping losses brings benefits such as longer range or alternatively, the possibility of reducing the amount of batteries while maintaining the same range at both a reduced battery weight and cost. Out of the two options, creating a vehicle with longer range is probably the most interesting design choice as it is a major focus for electrified vehicles, especially battery electric vehicles.

Since the results show that the designed cooling concept leads to a lower temperature in both the copper conductors and stator teeth, the heat transferred to the rotor and consequentially the magnets is decreased. Even though the concept doesn't directly cool the magnets, the fact that the cooling is closer to the rotor improves the situation for those as well. One big benefit of having a lower overall motor temperature during

operation is that the machine can act as buffer if the power demand would increase. It would take longer to heat up the machine to critical levels which means that the duration of maximum power output is increased. Improved cooling would also positively impact the continuous power curve as it is determined by the critical temperatures of the magnets and hairpin insulation.

As the concept increases the power density due to the reduced outer dimensions, it allows a greater design freedom. A smaller machine with the same performance can be used, giving more space to for example luggage, passengers or other technology. Another possibility when increasing the power density is to maintain the same external motor dimensions and thereby getting a more powerful electric machine, increasing the performance of the vehicle without the need of altering or moving the nearby structures which is both complex and costly.

The concept is shown to improve the performance, it does however come with a number of drawbacks which are relevant to highlight. One main drawback is the reduction in achievable copper fill rate. This study has not involved an investigation of how the performance of the electric machine compares to the reference. The concept achieves the same or higher fill rate as a wound stator but cannot reach the same rates as a comparable externally cooled hairpin solution. A thorough analysis should be made of how this difference in copper layout in the slot affects the machine. It should also be stated that this solution is more complex, probably has a higher cost and takes longer to produce than a conventionally cooled machine. This means that the cooling jacket has an advantage and since it is still an adequate solution it could be the best choice for some applications, especially outside of the automotive industry.

5.1 Environmental aspects

The increase in efficiency both due to the reduced copper losses in the machine as well as reduced pumping losses in the system is not only beneficial as it increases the range of the vehicle. It also has a positive impact on the environment. Even a small increase in efficiency for an electric vehicle can have a great impact due to the vast amount of vehicles worldwide. Using the electricity more efficiently leads to lower CO_2 emissions from the energy production, especially in regions that rely heavily on coal or oil for example. An increased efficiency also means that a lower amount of batteries will be needed in the car for a specific range. Battery production and especially the materials used are a big issue for electrified vehicles.

Another positive environmental impact is the reduction in material due to not needing the external housing of the cooling jacket. The estimated weight savings is around 1.5 kg. Less use of raw materials is beneficial in several ways. First of all the mining and refining of the material has a negative environmental impact. It also means reduced emissions from transportation of the raw material. It also brings down the weight of the overall vehicle which in turn can save more energy during operation.

Beyond the direct positive environmental impacts, it also improves the competitiveness of electrified vehicles against conventional combustion engine cars. All development that makes electrified vehicles more attractive to customers when it comes to aspects such as range and performance will lead to a faster transition towards electrification. Any increase in customer value of an electrified vehicle will drive the transition towards

more environmentally friendly transportation, provided that energy production moves towards more sustainable methods as well.

5.2 Future development

The more advanced CHT simulation should be further developed. By modelling the full machine with domains for each fluid region and component, including insulating layers, an estimation of for example internal magnet temperature can be made. This would be of great interest as this is a limiting factor of the power output of the machine. A moving reference frame should be applied to the rotor in order to account for the movement of the air caused by its rotation. After more thorough simulations have been performed, a prototype should be tested in order to verify the results.

The final design concept established in this report could be developed further by optimizing the flow path in the machine. In this study the design was improved by changing the channel geometry as well as the direction of the inlet and outlet. Once a viable design was determined it was not further optimized. The performance improvements seen by making small geometry changes in the concept shows the unoptimized state of the design. There are many more aspects that could and should be investigated and modified to improve the performance further. The cooling geometry could for example be designed to increase turbulence around the end regions to improve the heat transfer. Another aspect which has not been considered in this study is to minimize the coolant volume in the machine. A reduction in coolant is a reduction in weight as well as cost.

Another crucial step in the process of concept evaluation is to perform an analysis of how other aspects of the machine is affected by the alterations made. For example determining the efficiency map of the electric machine, estimating the continuous torque curve and simulating efficiency for different driving cycles. There are also several phenomena occurring in the electric machine that needs to be analysed such as back electromotive force (back EMF), which opposes the change in current, and torque ripple. One major change between the final concept and the reference machine that could affect the mentioned areas is the transition from windings to hairpins, the other components such as the stator, rotor and magnets have not been changed.

Sealing and insulation are two crucial aspects in order to achieve a reliable internally cooled machine, they should therefore be the main focuses when developing this concept further. The insulation and sealing principles should be developed to a higher degree with material selection and an analysis of required dimensions. After properly dimensioning the insulation the design should go through testing to ensure safe operation. The design must be robust, leakage of the coolant onto the hairpins, rotor or stator core is unacceptable and will lead to short circuit and machine failure. Another aspect that requires consideration during testing is if there is any occurrence of local boiling of the coolant since the rapid expansion due to boiling could cause damage to the machine. The occurrence of local boiling is however dependent on the coolant inlet temperature and for a BEV the temperature should be considerably lower than what has been used in this study. Corrosion is also an aspect which requires consideration when using a water and glycol mixture as coolant to guarantee the durability of the machine. If the insulation proves to be too difficult to achieve, the concept could use a dielectric coolant. Less insulation would be needed, however the coolant would have a lower specific heat capacity and most likely it would require a separate cooling circuit.

6 Conclusions

The main improvement area for the PMSM to increase power, efficiency and size is cooling. Internal cooling is determined to have the highest improvement potential for these criteria. Changing the cooling design of the electric machine results in a product with improved efficiency and power density while still being possible to mass produce. By using an internal cooling method with a hairpin solution, the outer geometry of the electric machine can be reduced by 8.8 % axially and 7.9 % radially. By removing the cooling jacket the housing weight is reduced by 1.5 kg. The size reduction enables design choices whether a smaller electric machine with maintained power is desired or higher power but keeping the original geometries. The performance of the internal cooling design over the cooling jacket is improved by decreasing the pressure drop by a factor of 7-8 and increasing the thermal duty by a factor of two. By having an internal cooling design the hairpin surface temperature can be reduced by up to around 92 %. The reduction in hairpin insulation temperature allows for an increased continuous power particularly in operating points with high torque and low engine speed where copper losses are dominant. An increased temperature would otherwise lead to the insulation overheating which can result in machine failure unless the current level and subsequently power output is reduced.

Changing to an internally cooled design increases the complexity compared to the cooling jacket. It is increased by the introduction of new components and assembly methods. It is concluded that dimensioning for durability require further investigation.

7 References

Andersson, B., 2013. *Lumped Parameter Thermal Modelling of Electric Machines,* Göteborg: Chalmers University of Technology.

Bejan, A., 2013. *Convection Heat Transfer (4th Edition).* Hoboken: John Wiley & Sons.

Benhaddadi, M., Olivier, G. & Ibtiouen, R., 2011. Chapter 1: Premium efficiency motors. In: M. Chomat, ed. *Electric Machines and Drives.* Rijeka: Intech, pp. 1-24.

Böckh, P. v. & Wetzel, T., 2012. *Heat Transfer.* 1 ed. Berlin Heidelberg: Springer.

Emgee, n.d.. *http://emgeecables.com/.* [Online] Available at: https://www.mcexpocomfort.it/__novadocuments/419356?v=636488256330530000 [Accessed 23 05 2019].

England, M. & Ponick, B., 2019. Automated Design of Hairpin Windings as Tabular Winding Diagrams. *e & i Elektrotechnik und Informationstechnik,* 136(2), pp. 159-167.

Grunditz, E. A., 2016. *Design and assessment of battery electric vehicle powertrain, with respect to performance, energy consumption and electric motor thermal capability* , Göteborg: Chalmers University of Technology.

Hussain, S. et al., 2016. *A study of the effects of temperature on magnetic and copper losses in electrical machines,* Lausanne: 2016 XXII International Conference on Electrical Machines (ICEM).

JinXin, F., ChengNing, Z., ZhiFu, W. & Strangas, E. G., 2010. Thermal analysis of water cooled surface mount permanent magnet electric motor for electric vehicle. *2010 International Conference on Electrical Machines and Systems,* pp. 1024-1028.

Johannesson, H., Persson, J.-G. & Pettersson, D., 2004. *Produktutveckling: Effektiva Metoder För Konstruktion Och Design.* 1st ed. Stockholm: Liber.

Kumar, A., 2018. *Electric motor internal heat convection modelling and analysis: Electric motor internal heat convection modelling and analysis,* Göteborg: Chalmers University of Technology .

Lindh, P. et al., 2017. Direct Liquid Cooling Method Verified With an Axial-Flux Permanent-Magnet Traction Machine Prototype. *IEEE Transactions on Industrial Electronics,* 64(8), pp. 6086-6095.

Liu, Z., Winter, T. & Schier, M., 2015. Direct Coil Cooling of a High Performance Switched Reluctance Machine (SRM) for EV/HEV Applications. *SAE Int. J. Alt. Power.*, 4(1), pp. 162-169.

Melkebeek, J., 2018. Small Synchronous Motors. In: *Electrical Machines and Drives.* Ghent: Springer International Publishing, pp. 489-522.

Menter, F., Kuntz, M. & Langtry, R., 2003. Ten years of industrial experience with the SST turbulence model. *Heat and Mass Transfer,* Volume 4, pp. 625-632.

Mital, A., Anoop, D., Anand, S. & Mital, A., 2008. Chapter 3 - The Structure of the Product Design Process. In: *Product Development.* Burlington: Elsevier Science & Technology, pp. 37-70.

Popescu, M. et al., 2013. Thermal Analysis of Duplex Three-Phase Induction Motor Under Fault Operating Conditions. *IEEE Transactions on Industry Applications,* 49(4), pp. 1523-1530.

Powell, R. C. & Buede, D. M., 2012. 8.1.4 Pugh Matrix.. In: *Project Manager's Guide to Making Successful Decisions.* Vienna: Management Concepts, Inc., pp. 191-192.

Project Management Institute, 2008. Chapter 2- Project Life Cycle and Organization. In: *A Guide to the Project Management Body Of Knowledge.* 4th ed. Newtown Square(Pennsylvania): Project Management Institute, Inc., pp. 15-36.

Pyrhonen, j., Jokinen, T. & Valeria, H., 2013. *Design of Rotating Electrical Machines.* 2nd ed. s.l.:John Wiley and Sons, Incorporated.

Schiefer, M. & Doppelbauer, M., 2015. Indirect slot cooling for high-power-density machines with concentrated winding. *2015 IEEE International Electric Machines & Drives Conference (IEMDC),* pp. 1820-1825.

Silverstein, D., Samuel, P. & DeCarlo, N., 2012. *Innovator's Toolkit - 50+ Techniques for Predictable and Sustainable Organic Growth.* 2nd ed. Hoboken: John Wiley & Sons, Inc.

Temco, 2017. *https://temcoindustrial.com.* [Online]
Available at: https://temcoindustrial.com/product-guides/wire-cable-and-accessories/magnet-wire/magnet-wire-faq
[Accessed 10 06 2019].

Tong, W., 2014. *Mechanical Design of Electric Motors.*. Boca Raton: CRC Press.

Vertsteeg, H. K. & Malalasekera, W., 2007. *An Introduction to Computational Fluid Dynamics.* 2nd ed. Harlow: Pearson Prentice Hall.

White, F. M., 2008. *Fluid Mechanics.* 6th ed. New York: McGraw-Hill.

Vivek, D. B., 2017. *Automotive Product Development.* 1st ed. Boca Raton: CRC Press.

Vukosavic, S. N., 2013. Chapter 4 - Magnetic Circuit. In: *Electrical Machines.* New York: Springer, pp. 59-80.

Xeu, S. et al., 2017. A New Iron Loss Model for Temperature Dependencies of Hysteresis and Eddy Current Losses in Electrical Machines. *IEEE Transactions on Magnetics,* 54(1), pp. 1-10.

Appendix A – Generated Concepts

Current solution	Concept 1 (Reference)	Concept 2	Concept 3	Concept 4
Epoxy resin	Method A	Method B	Method C	Method D
Solid laminat	Solid laminat	Solid laminat	Solid laminat	Solid laminat
Cooling jacket	End winding housing	No external stator cooling	No external stator cooling	No external stator cooling
Wire	Hairpin	Hairpin or rectangular	Hairpin	Hairpin
End winding epoxy resin	Fluid encapsulation	End winding epoxy resin	End winding epoxy resin	End winding epoxy resin
Side inlet	Fluid reservoir inlets	Manifold stator inlets	Manifold stator inlets	Manifold stator inlets
Side outlet	Fluid reservoir outlets	Manifold stator outlets	Manifold stator outlets	Manifold stator outlets
Water	Dielectric coolant (Water if insulated)	Water	Dielectric coolant	Water
Concept 5	**Concept 6**	**Concept 7**	**Concept 8**	**Concept 9**
Method A	Epoxy resin	Epoxy resin	Epoxy resin	Epoxy resin
Micro channels	Twisted channels	Axial channel	Exterior channels	Radial channel
End winding housing	No external stator cooling	No external stator cooling	Stator contact channel	No external stator cooling
Hairpin	Hairpin	Hairpin	Hairpin	Hairpin
Fluid encapsulation	End winding epoxy resin	End winding epoxy resin	End winding epoxy resin	End winding epoxy resin
Fluid reservoir inlets	Side inlet	Channel branching	Side inlet	Manifold stator inlets
Fluid reservoir outlets	Side outlet	Channel branching	Side outlet	Manifold stator outlets
Dielectric coolant	Dielectric coolant (Water if insulated)	Dielectric coolant (Water if insulated)	Dielectric coolant (Water if insulated)	Dielectric coolant (Water if insulated)
Concept 10	**Concept 11**	**Concept 12**	**Concept 13**	**Concept 14**
Epoxy resin	Method A	Method D	Method B	Epoxy resin
Exterior grooves	Axial channel	Solid laminat	Solid laminat	Solid laminat
Stator contact channel	End winding housing	Cooling jacket	Cooling jacket	Stator contact channel
Hairpin	Hairpin	Hairpin	Hairpin	Hairpin
End winding epoxy resin	Fluid encapsulation	End winding epoxy resin	End winding epoxy resin	Fluid jet
Side inlet	Fluid reservoir inlets	Side inlet + Manifold	Side inlet + Manifold	Side inlet +nozzle
Side outlet	Fluid reservoir outlets	Side outlet + Manifold	Side outlet + Manifold	Side outlet + fluid pan
Dielectric coolant (Water if insulated)	Dielectric coolant (Water if insulated)	Water	Water	Dielectric coolant

Figure A.1 List of the generated concepts (undefined methods due to confidentiality).

Appendix B – Pugh Matrices

	Concepts:	Current (ref)		1		2		3		4		5		6		7		8		9		10		11		12		13		14	
Criteria:	Weight	Value	Tot.	Value	Tot.	Value	Tot.	Value	Tot.	Value	Tot.	Value	Tot.	Value	Tot.	Value	Tot.	Value	Tot.	Value	Tot.	Value	Tot.	Value	Tot.	Value	Tot.	Value	Tot.	Value	Tot.
Efficiency	10	0	0	1	10	1	10	1	10	1	10	1	10	1	10	1	10	1	10	1	10	1	10	1	10	1	10	1	10	1	10
Continuous power	8	0	0	1	8	1	8	1	8	1	8	1	8	1	8	1	8	1	8	1	8	1	8	1	8	1	8	1	8	1	8
Size	8	0	0	1	8	1	8	1	8	1	8	1	8	1	8	1	8	1	8	1	8	1	8	-1	-8	-1	-8	-1	-8	-1	-8
Mass producibility	7	0	0	0	0	-1	-7	-1	-7	0	0	-1	-7	0	0	0	0	0	0	-1	-7	0	0	0	0	-1	-7	-1	-7	0	0
Quality	6	0	0	-1	-6	-1	-6	-1	-6	-1	-6	-1	-6	-1	-6	-1	-6	-1	-6	-1	-6	-1	-6	-1	-6	-1	-6	-1	-6	-1	-6
Cost	5	0	0	0	0	-1	-5	-1	-5	0	0	0	0	0	0	0	0	0	0	0	0	0	0	0	0	0	0	-1	-5	-1	-5
Complexity	3	0	0	-1	-3	-1	-3	-1	-3	-1	-3	-1	-3	-1	-3	-1	-3	-1	-3	-1	-3	-1	-3	-1	-3	-1	-3	-1	-3	-1	-3
Weight	1	0	0	1	1	1	1	1	1	1	1	1	1	1	1	1	1	1	1	1	1	1	1	1	1	-1	-1	-1	-1	-1	-1
Environmental aspects	4	0	0	1	4	1	4	1	4	1	4	1	4	1	4	1	4	1	4	1	4	1	4	1	4	0	0	1	4	0	0
Structural properties	2	0	0	-1	-2	-1	-2	-1	-2	-1	-2	-1	-2	-1	-2	-1	-2	-1	-2	-1	-2	-1	-2	0	0	0	0	0	0	-1	-2
Total Score			0		20		8		8		20		13		20		20		20		13		20		-7		-8		-7		

Figure B.1 Weighted Pugh matrix with current solution as reference.

Concepts:		1 (Ref)		2		3		4		5		6		7		8		9		10		11		Current	
Criteria:	Weight	Value	Tot.	Value	Tot.	Value	Tot.	Value	Tot.	Value	Tot.	Value	Tot.	Value	Tot.	Value	Tot.	Value	Tot.	Value	Tot.	Value	Tot.	Value	Tot.
Efficiency	10	0	0	-1	-10	0	0	-1	-10	0	0	-1	-10	-1	-10	-1	-10	-1	-10	-1	-10	0	0	-1	-10
Continuous power	8	0	0	-1	-8	0	0	-1	-8	1	8	-1	-8	-1	-8	-1	-8	-1	-8	-1	-8	1	8	-1	-8
Size	8	0	0	0	0	1	8	0	0	0	0	1	8	1	8	0	0	1	8	0	0	0	0	-1	-8
Mass producibility	7	0	0	-1	-7	-1	-7	0	0	-1	-7	0	0	0	0	0	0	-1	-7	0	0	0	0	0	0
Quality	6	0	0	0	0	-1	-6	1	6	0	0	0	0	0	0	1	6	0	0	0	0	0	0	1	6
Cost	5	0	0	-1	-5	-1	-5	0	0	0	0	0	0	0	0	0	0	0	0	0	0	0	0	0	0
Complexity	3	0	0	-1	-3	-1	-3	-1	-3	-1	-3	1	3	1	3	1	3	0	0	1	3	0	0	1	3
Weight	1	0	0	1	1	1	1	0	0	0	0	1	1	1	1	0	0	1	1	1	1	0	0	-1	-1
Environmental aspects	4	0	0	-1	-4	0	0	-1	-4	0	0	-1	-4	-1	-4	0	0	-1	-4	-1	-4	0	0	-1	-4
Structural properties	2	0	0	0	0	0	0	0	0	-1	-2	0	0	0	0	0	0	0	0	0	0	-1	-2	1	2
Total Score			0		-36		-12		-19		-4		-10		-10		-9		-20		-18		6		-20

Figure B.2 Weighted Pugh matrix with concept 1 as reference.